Molecular Structure of Substituted Phenylamine α-OMe- and α-OH-*p*-Benzoquinone Derivatives. Synthesis and Correlation of Spectroscopic, Electrochemical, and Theoretical Parameters

M. Aguilar-Martínez,*[,†,‡] J. A. Bautista-Martínez,[†] N. Macías-Ruvalcaba,[†] I. González,[§] E. Tovar,[†] T. Marín del Alizal,[‖] O. Collera,[†] and G. Cuevas[†]

Universidad Nacional Autónoma de México, Instituto de Química, Ciudad Universitaria, 04510 México D.F., México, Universidad Autónoma Metropolitana-Iztapalapa, Departamento de Química, Apartado postal 55-534, 09340 México D.F., Mexico, and Universidad la Salle, Escuela de Ciencias Químicas, Benjamin Franklin 47, Hipódromo Condesa, 06140 México D.F., Mexico

marthaa@servidor.unam.mx

Received March 19, 2001

Thirteen C_6 para-substituted anilinebenzoquinones derived from perezone (PZ) (2-(1,5-dimethyl-4-hexenyl)-3-hydroxy-5-methyl-1,4-benzoquinone) were prepared to analyze the effect of the substituents on quinone electronic properties. The effect of a hydrogen bond between the α-hydroxy and carbonyl C_4-O_4 groups was determined in perezone derivatives by substituting electron-donor and electron-acceptor groups such as −OMe, −Me, −Br, and −CN and comparing the −OH (APZs) and −OMe (APZms) derivatives. Reduction potentials of these compounds were measured using cyclic voltammetry in anhydrous acetonitrile. The typical behavior of quinones, with or without α-phenolic protons, in an aprotic medium was not observed for APZs due to the presence of coupled, self-protonation reactions. The self-protonation process gives rise to an initial wave, corresponding to the irreversible reduction reaction of quinone (HQ) to hydroquinone (HQH_2), and to a second electron transfer, attributed to the reversible reduction of perezonate (Q^-) formed during the self-protonation process. This reaction is favored by the acidity of the α-OH located at the quinone ring. To control the coupled chemical reaction, we considered both methylation of the −OH group (APZms) and addition of a strong base, tetramethylammonium phenolate ($Me_4N^+C_6H_5O^-$), to completely deprotonate the APZs. Methylation led to recovery of reversible, bi-electronic behavior ($Q/Q^{\bullet -}$ and $Q^{\bullet -}/Q^{2-}$), indicating the nonacidic properties of the NH group. The addition of a strong base resulted in reduction of perezonate (Q^-) obtained from the acid−base reaction of APZs with $Me_4N^+C_6H_5O^-$ to produce the dianion radical ($Q^{\bullet 2-}$). Although the nitrogen atom interferes with direct conjugation between both rings by binding the quinone with the para-substituted ring, the UV−vis spectra of these compounds showed the existence of intramolecular electronic transfer from the respective aniline to the quinone moiety. ^{13}C NMR chemical shifts of the quinone atoms provided additional evidence for this electron transfer. These findings were also supported by linear variation in cathodic peak potentials (E_{pc}) vs Hammett σ_p constants associated with the different electrochemical transformations: $Q/Q^{\bullet -}$, $Q^{\bullet -}/Q^{2-}$ for APZms or HQ/HQH_2 and $Q^-/Q^{\bullet 2-}$ for APZs. The electronic properties of model anilinebenzoquinones were determined at a B3LYP/6-31G(d,p) level of theory within the framework of the density functional theory. Our theoretical calculations predicted that all the compounds are floppy molecules with a low rotational C−N barrier, in which the degree of conjugation of the lone nitrogen pair with the quinone system depends on the magnitude of the electronic effect of the substituents of the aniline ring. Natural charges show that C_1 is more positive than C_4 although the LUMO orbital is located at C_4. Hence, if the natural charge distribution in the molecule controls the first electron addition, this should occur at carbon atom C_1. If the process is controlled by the LUMO orbitals, however, electron addition would first occur at C_4. For the APZms series susceptibility of the first reduction wave to the substitution effect ($\rho_\pi = 147$ mV) is lower than that of the second reduction wave ($\rho_\pi = 156$ mV). Thus, the first, one-electron transfer in the quinone system is controlled by the natural charge distribution of the molecule and therefore takes place at C_1.

Introduction

Quinones are found in all respiring animal and plant cells where they function primarily as components of the electron transport chains involved in cellular respiration[1] and photosynthesis.[2] These compounds occur in other natural contexts[3] and as pollutants.[3,4] Quinones form an important class of toxic metabolites and, paradoxically,

[†] Universidad Nacional Autónoma de México.
[‡] On leave from Universidad Nacional Autónoma de México, Facultad de Química, Departamento de Fisicoquímica, Ciudad Universitaria, 04510 México D.F., México.
[§] Universidad Autónoma Metropolitana-Iztapalapa.
[‖] Universidad la Salle.

(1) Morton, R. A., Ed. *Biochemistry of Quinones*; Academic Press: New York, NY, 1965.
(2) (a) Bentley, R.; Campbell, I. M. In Patai, S. Ed. *The Chemistry of Quinoid Compounds*; John Wiley & Sons: London, 1974; pp 683−736. (b) Nohl, H.; Jordan, W.; Youngman, R. J. *Adv. Free Radical Biol. Med.* **1986**, *2*, 211−279.
(3) Monks, T. J.; Hanzlik, R. P.; Cohen, G. M.; Ross, D.; Graham, D. G. *Toxicol. Appl. Pharmacol.* **1992**, *112*, 2−16.

10.1021/jo010302z CCC: $20.00
Published on Web 11/08/2001

can be either mutagenic and, therefore, potentially carcinogenic, or effective anticancer agents.[5] Some quinones possibly play a role in cellular defense since they effectively inhibit growth of bacteria,[6] fungi,[7] or parasites.[8]

A variety of biologically active, naturally occurring quinones with such properties[9] contain acidic hydrogens in their structure, and many are more active than quinones lacking acidic hydrogens. Such anticancer drugs as adriamycin, daunorubicin, streptonigrim, lapachol, and their analogues contain quinones with hydroxyl groups.[10] Methylation of either or both of the α-hydroxyl groups of the quinone carbonyl groups in the anticancer agent, daunomycin, results in a significant reduction in antitumor effects.[11] This could be due to greater difficulty in semiquinone formation resulting from obstruction of the hydroxyl groups by methylation.[12,13]

Some hydroxynaphthoquinones were found to have higher trypanocidal activity than quinones lacking the −OH group.[14] Measurements of the corresponding methoxy and acetoxyquinones[11] indicate that internal hydrogen bonding in the α-hydroxyquinones contributes to stabilization of the semiquinone, probably as a result of increased delocalization due to exchange of the hydroxyl hydrogen between the two neighboring oxygen atoms. Hydroxyl-substituted derivatives of antineoplastic furanquinones capable of internal hydrogen bonding exhibit the most positive $E_{1/2}$ values and are generally more active than unsubstituted counterparts.[15]

Biological activity is closely related to the redox and acid−base chemistry of the quinones, semiquinones, and hydroquinones. The ability as electron donors or acceptors of the substituents present in quinones significantly alters their acid−base properties. To understand how quinones function in such varied and crucial biochemical roles, it is important to evaluate the effect of the substituents on the electrochemical behavior of α-hydroxyquinones.

The electrochemical behavior of different quinones is extensively reviewed.[16] The effects of quinone substituents have been described for molecules without functional acidic groups[17] or within a family of quinones with α-hydroxiphenolic groups that lack electron-accepting or -donating substituents.[18,19,20] Several reports[21,22] consider the effect of the substituents on the electrochemical properties of quinone families that have an α-phenolic group. In such quinones, the intramolecular hydrogen bonding stabilizes the semiquinone radical and two, one-electron reversible reduction processes are maintained despite the hydrogen bond presence.[19,20] However, in these molecules, the α-OH groups at the quinone rings are more acidic than those of the phenolic group. Thus, electrochemical behavior of the α-hydroxy quinones is more irreversible than that of the phenolic quinones due to the transfer of the hydrogen bonding proton during electron addition.[18,22,23]

Since quinones containing more acidic protons, such as the α-hydroxyquinones, display different electrochemical behavior[17,23] than quinones without them, we were interested in studying the effect of the substituents on the electrochemical properties of a family of quinones containing an α-hydroxy group in its structure, the anilineperezones APZs, and comparing their behavior with that of their methylated quinones (APZms, Table 1). Using these anilines allowed us to control modification of the effect of the substituents on the redox potential of the quinone system. In previous electrochemical reduction studies of a group of quinone molecules lacking acidic hydrogen, the 2-[(R-phenyl)amine]-1,4-naphthalenediones in acetonitrile, we found that half-wave potential values varied linearly with the electronic effect of the substituents.[24] We also observed that the nitrogen from the aniline group softened the electronic effect of the substituents.

In addition to substituent effects, the redox and acid−base equilibrium properties of quinones are also modified by controlling media acidity. Control of pH is important for those compounds where self-protonation can occur since a more acid environment modifies the quantity of quinone transformed to hydroquinone. Diminished quinone transformation occurs since some molecules are involved in protonation of the electrochemical reduction products, leaving a smaller number of molecules to participate in the electron-transfer process.[25] In this work, the strong base, tetramethylammonium phenolate

(4) (a) Fox, M. A.; Olive, S. *Science* **1979**, *205*, 582−583. (b) Pryor, W. A.; Hales, B. J.; Premivic, P. I.; Church, D. F. *Science* **1982**, *220*, 425−427.

(5) Lin, A. J.; Cosby, L. A.; Sartorelli, A. C. *Cancer Chemother. Rep. Part 2* **1974**, *4*, 23−25.

(6) Hoover, J. R. E.; Dag, A. R. *J. Am. Chem. Soc.* **1954**, *76*, 4148−4152.

(7) (a) Rich, S. In *Fungicides, An Advanced Treatise*; Torgeson, D. C., Ed.; Academic Press: New York, 1969. (b) Clark, N. G. *Pestic. Sci.* **1985**, *16*, 23−32.

(8) Howland, J. L. *Biochim. Biophys. Acta* **1963**, *73*, 665−667.

(9) (a) Inbaraj, J. J.; Gandhidasan, R.; Murugesan, R. *Free Radical Biol. Med.* **1999**, *26*, 1072−1078. (b) Frigaard, N. U.; Tokita, S.; Matsuura, K. *Biochim. Biophys. Acta* **1999**, *1413*, 108−116. (c) Rodríguez Hahn, L.; Esquivel, B.; Sánchez, A. D.; Sánchez, C.; Cárdenas, J.; Ramamoorthy, T. P. *Rev. Latinoamer. Quim.* **1989**, *20*, 105−113. (d) Pezzuto, J. M.; Fong, H. H. S.; Farnsworth, N. R.; Che, C. T. *J. Nat. Prod.* **1989**, *52*, 571−575. (e) Inbaraj, J. J.; Krishna, M. C.; Gandhidasan, R.; Murugesan, R. *Biochim. Biophys. Acta* **1999**, *1413*, 462−470.

(10) Bachur, N. R.; Gordon, S. L.; Gee, M. V. *Cancer Res.* **1978**, 1745−1750.

(11) Ashnagar, A.; Bruce, J. M.; Dutton, P. L.; Prince, R. C.*Biochim. Biophys. Acta* **1984**, *801*, 351−359.

(12) Rao, G. M.; Lown, J. W.; Plambeck, J. A. *J. Electrochem. Soc.* **1978**, *125*, 534−539.

(13) Rao, G. M.; Lown, J. W.; Plambeck, J. A. *J. Electrochem. Soc.* **1978**, *125*, 540−543.

(14) Goulart, M. O. F.; Zani, C. L.; Tonholo, J.; Freitas, L. R.; de Abreu, F. C.; Oliveira, A. B.; Raslan, D. S.; Starling, S.; Chiari. E. *Bioorg. Med. Chem. Lett.* **1997**, *7*, 2043−2048.

(15) Crawford, P. W.; Carlos, E.; Ellegood, J. C.; Cheng, C. C.; Dong, Q.; Liu, D. F.; Luo, Y. L. *Electrochim. Acta* **1996**, *41*, 2399−2403.

(16) (a) Chambers, J. Q. Electrochemistry of Quinones. In *The Chemistry of Quinonoid Compounds. Vol II*; Patai, S., Rappoport, Z., Eds.; John Wiley and Sons, Ltd.: New York, 1988; Chapter 12. (b) Bard, A. J.; Faulkner, L. R. *Electrochemical Methods. Fundamentals and Applications*; John Wiley & Sons, Inc.: New York, 1980. (c) Evans, D.; Laviron, E. *J. Electroanal. Chem.* **1986**, *208*, 357−372.

(17) (a) Glezer, V.; Turovska, B.; Stradins, J.; Freimanis, J. *Electrochim. Acta* **1990**, *35*, 1933−1940. (b) Illescas, B.; Martín, N.; Segura, J. L.; Seoane, C.; Ortí, E.; Viruela, P. M.; Viruela, R. *J. Org. Chem.* **1995**, *60*, 5643−5650.

(18) González, F. J.; Aceves, J. M.; Miranda, R. And González, I. *J. Electroanal. Chem.* **1991**, *310*, 293−303.

(19) Wightman, R. M.; Cockrell, J. R.; Murria, R. W.; Burnett, J. N.; Jones, S. B. *J. Am. Chem. Soc.* **1976**, *98*, 2562−2570

(20) Piljac, I.; Murray, R. W. *J. Elecetrochem. Soc.* **1971**, *118*, 1758−1764.

(21) Li, C.-Y.; Caspar, M. L.; Dixon, D. W. *Electrochim. Acta* **1980**, *25*, 1135−1142.

(22) Edwards, T. G.; Grinter, R. *Trans. Faraday Soc.* **1968**, *69*, 1070−1076.

(23) Ortiz, J. L.; Delgado, J.; Baeza, A.; Gonzáles, I.; Sanabria, R.; Miranda, R. *J. Electroanal. Chem.* **1996**, *411*, 103−107.

(24) Aguilar-Martínez, M.; Cuevas, G.; Jiménez-Estrada, M.; González, I.; Lotina-Hessen, B.; Macías-Ruvalcaba, N. *J. Org. Chem.* **1999**, *64*, 3684−3694.

(25) Amatore, C.; Capobianco, G.; Farnia, G.; Sandonà, G.; Savéant, J. M.; Severin, M. G.; Vianello, E. *J. Am. Chem. Soc.* **1985**, *107*, 1815−1824.

Table 1. Structure of (2-(1,5-Dimethyl-4-hexenyl)-3-hydroxy-5-methyl-6-[4′-(R_2-phenyl)amine]-1,4-benzoquinones (APZs) and Their 3-Methoxy Derivatives (R_1 = Me) Synthesized in This Work

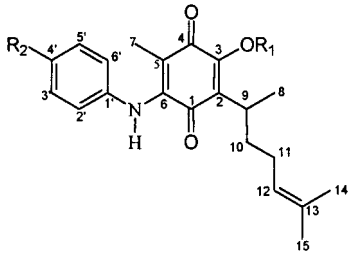

compd	R_1	R_2
APZ	−H	−H
p-MeOAPZ	−H	$-OCH_3$
p-BrAPZ	−H	−Br
p-MeAPZ	−H	$-CH_3$
p-CNAPZ	−H	−CN
p-MeCOAPZ	−H	$-COCH_3$
p-NO_2APZ	−H	$-NO_2$
APZm	$-CH_3$	−H
p-MeOAPZm	$-CH_3$	$-OCH_3$
p-BrAPZm	$-CH_3$	−Br
p-MeAPZm	$-CH_3$	$-CH_3$
p-CNAPZm	$-CH_3$	−CN
p-MeCOAPZm	$-CH_3$	$-COCH_3$
p-NO_2APZm	$-CH_3$	$-NO_2$

($Me_4N^+C_6H_5O^-$), was added to avoid the self-protonation reaction.

Electrochemical studies of compounds are generally performed in aqueous solutions under conditions close to physiological pH 7 to reproduce their native biological activity. However, some biological electron-transfers occur in the lipid phase.[26] Thus, it is important to determine the electrochemical behavior of these compounds in aprotic solvents in order to mimic the cells nonpolar environment.[11,15,27]

We report the synthesis, characterization, X-ray analysis, and electrochemical behavior of PZ and 2-(1,5-dimethyl-4-hexenyl)-5-methyl-3-methoxy-1,4-benzoquinone (PZm) (Figure 1) and their 6-(4′-R-phenyl)amine derivatives APZs and APZms (Table 1) in acetonitrile and present a theoretical analysis for a molecular model of these quinones.

Results and Discussion

Synthesis. Perezone derivatives (Table 1) were prepared by addition of the corresponding para-substituted aniline in anhydrous THF to an equimolar solution of PZ[28,29] (**1**, Figure 2), under nitrogen atmosphere. Methylated derivatives (**3**, Figure 2) were obtained by adding an anhydrous dimethyl sulfate solution in dry acetone to the previously prepared perezone adducts[30] (**2**, Figure 2). Yields were notably improved when the aniline was introduced to the perezone first and then methylated rather than performing the methylation first.

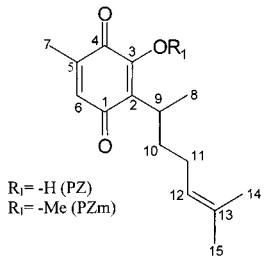

Figure 1. Structures of (2-(1,5-dimethyl-4-hexenyl)-3-hydroxy-5-methyl-1,4-benzoquinone (PZ) and (2-(1,5-dimethyl-4-hexenyl)-3-methoxy-5-methyl-1,4-benzoquinone (PZm).

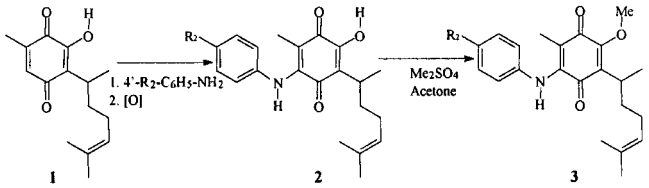

Figure 2. Synthesis of APZs and APZms.

This difference in yield may be due to the polarization effect of the OH group on the quinone carbonyl through a hydrogen bond that is susceptible to a Michael-type addition at the C_6 position. The derivatives obtained with the first method varied in color from purple (substituents with the methoxy group) to red (substituents with the nitro group).

Spectroscopy. In methanol, these quinones display some common absorption bands that concur with our interests, such as one in the 204−211 nm region assigned to the intense benzene and quinone $\pi-\pi^*$ transition. In the 313−361 nm region, there is a transfer band and a very broad, low energy band at 449−543 nm due to the $n-\pi^*$ transition of the carbonyl groups of the quinones. Some quinones show specific absorptions originating from the aniline substituents and will not be discussed in this paper.

The λ_{max} corresponding to the $n-\pi^*$ transition has interesting shifts depending on the nature of the substituents. Electron-donor groups cause a change in absorption at higher wavelengths for both hydroxylated (R_1 = −OH) and methylated derivatives (R_1 = −OMe), while electron-accepting groups cause the opposite effect. The graph of $1/\lambda_{max}$ for the $n-\pi^*$ transition for each series of compounds vs the Hammett constant[31] (σ_p) shows a linear correlation for the methylated derivatives (eq 1), but this linearity does not persist for the hydroxylated compounds (eq 2).

$$1/\lambda_{max}\,(nm^{-1})_{APZms} = 1.64 \times 10^{-4}\sigma_p + 1.9 \times 10^{-3} \quad (n = 7,\ r = 0.99) \quad (1)$$

$$1/\lambda_{max}\,(nm^{-1})_{APZs} = 4.04 \times 10^{-5}\sigma_p + 1.9 \times 10^{-3} \quad (n = 7,\ r = 0.42) \quad (2)$$

These data show that even if there is no direct conjugation between the substituents at position 4′ on

(26) Weiss, H.; Friedrich, T.; Hofhaus, G.; Preis, D. *Eur. J. Biochem.* **1991**, *197*, 563.

(27) (a) Li, C.-Y.; Jenq, J. *Electrochim. Acta* **1991**, *36*, 269−276. (b) Crawford, P. W.; Gross, J.; Lawson, K.; Cheng, C. C.; Dong, Q.; Liu, D. F.; Luo, Y. L.; Szczepankiewicz, B. G.; Heathcock, C. H. *J. Electrochem. Soc.* **1997**, *144*, 3710−3715. (c) Jeziorek, D.; Ossowski, T.; Liwo, A.; Dyl, D.; Nowacka, M.; WoŸnicki, W. *J. Chem. Soc., Perkin Trans. 2* **1997**, 229−236.

(28) Walls, F.; Salmón, M.; Padilla, J.; Joseph-Nathan, P.; Romo, J. *Bol. Inst. Quím. Univ. Nac. Auton. Mex.* **1965**, *17*, 3−15.

(29) Kögl, F.; Boer, A. G. *Rec. Trav. Chim. Pays-Bas* **1935**, *54*, 779−794.

(30) Rodríguez-Hernández, A.; Barrios, H.; Collera, O.; Enríquez, R. G.; Ortiz, B.; Sánchez Obregón, R.; Walls, F.; Yuste, F.; Reynolds, W. F.; Yu, M. *Nat. Prod. Lett.* **1994**, *4*, 133−139.

(31) Ewing, D. F. in Chapman, N. B. *Shorter Correlation Analysis in Chemistry: Recent Advances*; Plenum: New York, 1978; pp 357−396 and references therein.

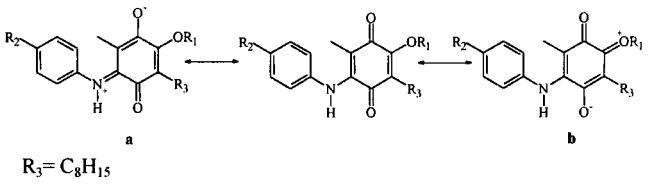

Figure 3. Dominant hybrids of APZs and APZms showing: (a) donation of electrons from the nitrogen atom to the segment $C_6-C_5-C_4-O_4$ and (b) donation of electrons from the oxygen atom to the segment $C_3-C_2-C_1-O_1$.

the aromatic ring and the quinone, the effects are transmitted through the nitrogen atom connecting these two moieties (Figure 3a). The σ_p values used in this study correspond to the standard Hammett values.[32]

Loss of linearity for the hydroxylated derivatives is more accentuated for electron-donor groups (−OMe, −Me). The elimination of these points improves the correlation (eq 3).

$$1/\lambda_{max}\,(nm^{-1})_{APZs} = 1.36 \times 10^{-4}\sigma_p + 1.9 \times 10^{-3} \quad (n = 5,\ r = 0.92) \quad (3)$$

This spectroscopic behavior is probably due to the hydroxyl group polarizing the C_4-O_4 carbonyl intensifying the methoxy and methyl groups donor properties. This is not possible when R_1 is a methyl group, as this group is incapable of improving the acceptor properties of the carbonyl. This effect then occurs because the electron-donor capabilities of the −OMe and −Me groups in the APZm series are saturated. The hydrogen bridge modifies the donor properties of the substituents that impact this correlation.

Nuclear magnetic resonance is very sensitive to the electronic effect of the substituents.[33] The Hammett equation applies to many physical measurements including infrared frequencies and NMR chemical shifts.[31] Plotting the chemical shift (δ) values obtained for each carbon atom of every compound (see the Experimental Section) against the σ_p Hammett substituent[32] constants produced a linear correlation (Table 2), where the slope is a measure of sensitivity of the chemical shift to electronic substituent effects. For the APZ series, the group that deviates from the linear correlation is −CN in all cases and the −CN and −Me groups for the C_2. The same is described for each anomalous substituent in the APZm derivatives. Because of their low steric volume and the small polarization capabilities of some groups, it is difficult to explain the origin of the effect on the observed chemical shift in terms of special donor properties or solvation.

In the ^{13}C NMR spectra, carbonyl groups of the quinoid ring show marked sensitivity to the effect of the substituents even if they are located up to nine bonds away from the group that originates the perturbation (Table 2). As expected, no substituent effect was observed on the saturated carbons of the lateral chain. In contrast, the carbons at positions 5 and 6 and the methyl on the quinone are the most sensitive to the effect of the substituents.[34]

Table 2. Correlation between Chemical Shifts (δ) with the Hammett Constant (σ_p) of (2-(1,5-Dimethyl-4-hexenyl)-3-hydroxy-5-methyl-6-[4′-(R_2-phenyl)amine]-1,4-benzoquinones (APZs) and (2-(1,5-Dimethyl-4-hexenyl)-3-methoxy-5-methyl-6-[4′-(R_2-phenyl)amine]-1,4-benzoquinones (APZms)

$\delta = \rho_\pi\sigma_p + b$
with n molecules in the correlation and r correlation coefficient

APZs					APZms				
carbon	ρ_π	b	n	r	carbon	ρ_π	b	n	r
C_1	0.31	182.80	6	1[a]	C_1	−0.52	184.95	7	0.97
C_2	5.41	126.74	5	1[a,b]	C_2	1.33	131.70	6	0.99[c]
C_3	−0.45	153.60	6	1[a]	C_3	−0.58	158.04	7	0.99
C_4	0.60	181.97	6	1[a]	C_4	0.28	183.18	5	0.96[d]
					C_4	0.29	183.20	7	0.90
C_5	0.94	118.76	6	1[a]	C_5	7.99	112.39	6	0.99[a]
C_6	−0.41	143.06	6	1[a]	C_6	5.86	140.62	6	0.90[e]
C_7	1.06	11.82	6	1[a]	C_7	1.55	12.49	7	0.98
C_{12}	−0.54	124.95	6	1[a]	C_{12}	−0.21	124.51	6	0.98
C_{13}	0.13	130.96	6	1[a]	C_{13}	0.25	131.46	6	0.99[f]
					C_{13}	0.29	131.45	7	0.75

[a] Without the group −CN. [b] Without the group −Me. [c] Without the group −Br. [d] Without the groups −CN and −H. [e] Without the group −MeO. [f] Without the group −H.

Sensitivity of the carbon atom of the quinone methyl group (C_7) to the effect of the substituent is interesting since the carbon atom can only participate in this process through hyperconjugation. In the APZm derivatives (Table 1), in ^1H NMR the methyl group at C_5 varies its chemical shift from 1.56 ppm (R_2 = −OMe) to 1.69 ppm (R_2 = $-NO_2$). However, there is no linear correlation between this shift and the σ_p value. This effect is similar for the APZ derivatives and suggests that when the quinone ring is substituted by electron-donor groups, the hydrogen atoms involved in the hyperconjugative interaction gain charge in the electron-transfer process.

In the APZ series, the C_2 carbon is more sensitive to the effect of the substituents than the same carbon on the methylated derivatives. This can be observed by the lower slope value for the methylated derivatives (Table 2). The positive slope implies that the electron-accepting substituents produce a low field chemical shift. These results demonstrate the greater donor capability of the hydroxy group with respect to the methoxy group and that this electron donation is favored when the ring substituent is an electron-donor. The values in Table 2 show that C_1 is less sensitive to the effect of the substituent than C_4.

The high field shift of C_4 is likely due to compensation of the low electronic density associated with the carbonyl atom by the donor capability of the nitrogen atom. This capability is decreased by electron-accepting substituents. The effect is more remarkable for the APZ than APZm series due to greater polarization of the carbonyl group originated by the hydrogen bridge.

The carbonyl atom C_1 in the APZm series behaves in the opposite manner, where electron-accepting groups produce the high field chemical shift. This effect has its origin in the different acidic properties of the hydrogen atom attached to nitrogen. The nitro group increases hydrogen acidity and the strength of the N−H···O hydrogen bridge, diminishing electronic density of the carbonyl atom. The reverse occurs for the methoxy group at C_3. The OH group at C_3 of the APZ series attenuates

(32) Hansch, C.; Leo, A.; Taft, R. W. *Chem. Rev.* **1991**, *91*, 165−195.

(33) (a) Derome, A. E. *Modern NMR Techiques for Chemistry Research*; Pergamon Press: Oxford, 1987. (b) Sanders, J. K. M.; Hunter, B. K. *Modern NMR Spectroscopy. A Guide for Chemists*; Oxford University Press: Oxford, 1987.

(34) This numbering is in agreement with Scheme 1 in Table 1.

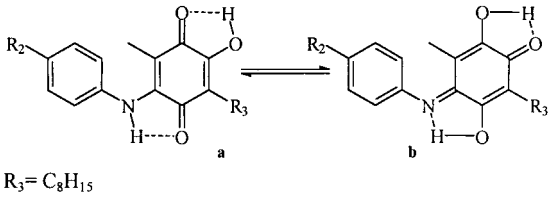

Figure 4. Hydrogen bondings showing the electronic communication between the enone segments.

this effect by direct conjugation and the balance of both influences produces a similar trend for C_4.

Carbons C_2 and C_5 in both series experience low field chemical shifts when effective donor groups are substituted by groups with poor donor character. This shift is associated to charge depletion and agrees with the resonant structures shown in Figure 3. On the other hand, a similar resonant structure explains the high field chemical shift of the ^{13}C NMR signals of C_3 and C_6 in both series originated by the oxygen atom attached to C_3.

The results of both UV−vis and ^{13}C NMR spectra indicate that two resonant forms are relevant in the stabilization of the hydroxylated derivatives. One of these is generated by donation of the nitrogen atom to the quinone ring and the other by donation of the oxygen atom (of the hydroxyl group) to the quinone connected by the hydrogen bridge (Figures 3a and 3b, respectively). Substituents that increase the electron-donor capacity of the nitrogen atom (electron-donor substituents) favor participation of the oxygen atom.

In the ^{13}C NMR spectra, the C_4 carbon shifts to a higher field than the C_1 carbon. The $\Delta\delta$ varies depending on electronic properties of the substituents and on donor properties of the −OH group compared to the −OMe group. These effects are likely due to the overall lower donor capacity of the −OMe group decreasing the protective effect at C_1. On the other hand, the amino group has a protective effect at C_4 that increases through participation of a hydrogen bonding OH···O_3−C_3 to polarize the carbonyl fragment and facilitate the $n_N \rightarrow \pi^*$ electronic interaction.

The resonant forms described in Figure 3 are based on these experimental observations and allow us to establish that the hydrogen bond serves as electronic communication between the enone segments in the quinone (Figure 4). Structure b in Figure 4 represents one extreme of this effect.

Greater sensitivity is observed in the unsaturated carbons on the side chain of the PZ. In both series (R_1 = −OH, R_1 = −OMe), the sign of ρ_π differs with the more substituted carbon atom having a positive sign (Table 2). Such sensitivity can only be explained in terms of an interaction of the charge transference complex between the double bond and the quinoid ring in solution. The explanation for this observation will be pursued in a subsequent study.

Electrochemistry. The redox potentials of the aniline-perezones APZs and APZms determined in this work were measured by cyclic voltammetry at 25 °C controlled temperature using a glassy carbon electrode in acetonitrile solvent and tetraethylammonium tetrafluoroborate as the supporting electrolyte. The voltammograms were recorded in the potential range from 250 to −2500 mV vs Fc/Fc^+.

Electrochemical Behavior of APZm Derivatives. Figure 5a shows the typical electrochemical behavior of

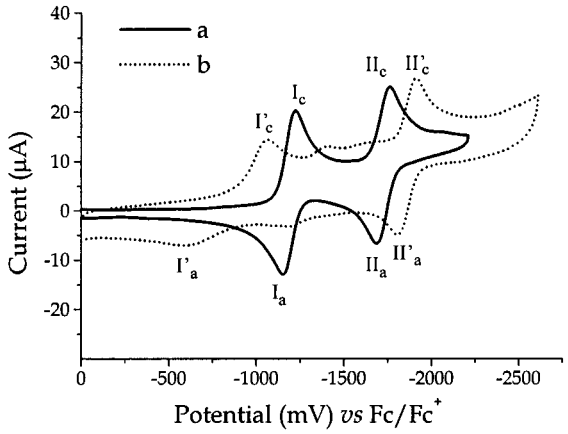

Figure 5. Typical cyclic voltammograms obtained with a glassy carbon electrode (7 mm^2), scan rate 100 mVs^{-1} in 0.1 M Et_4NBF_4/acetonitrile in the presence of the corresponding quinone 1 mM: (a) *p*-MeAPZm and (b) *p*-MeAPZ. The cathodic (I_c, II_c and I'_c, II'_c) and anodic (I_a, II_a and I'_a, II'_a) peaks are indicated.

APZm series which proceeded in two, one-electron diffusion stages, waves I and II (mechanism EE):

$$\mathrm{APZm} + e^- \rightleftarrows \mathrm{APZm}^{\bullet -} \quad (4)$$

$$\mathrm{APZm}^{\bullet -} + e^- \rightleftarrows \mathrm{APZm}^{2-} \quad (5)$$

The same behavior was observed within the sweep potential range of 50−1000 mVs^{-1}. At scan rates above 1000 mVs^{-1}, however, small distortions were detected in the cyclic voltammograms confounding determination of the corresponding electrochemical parameters. In our discussion of the results, we therefore dealt only with data obtained between 100 and 1000 mVs^{-1}. The half-wave potential values, $E_{1/2}$, for both waves were evaluated from the voltammograms obtained at a sweep rate of 100 mVs^{-1}, where $E_{1/2} = (E_{pa} + E_{pc})/2$ and E_{pa} and E_{pc} correspond to the anodic and cathodic peak potentials for each wave. However, for comparative purposes with the APZ series, where determination of $E_{1/2}$ was not possible, we used the cathodic peak potential for peak I (E_{pcI}) values at 100 mV s^{-1} for APZms and APZs. In all APZms, the cathodic peak current (i_{pc}) vs the square root of the sweep rate ($v^{1/2}$), produced a linear relationship with zero intercept for both peaks indicating the lack of detectable chemical kinetic complications.[26] Consistent voltammetric function ($i_{pc}v^{-1/2}c^{-1}$) with the logarithm of the sweep rate confirmed this behavior. The $i_{pc}v^{-1/2}c^{-1}$ values are reported in Table 3. Voltammetric function values were standardized for concentration and reported as $i_{pc}v^{-1/2}c^{-1}$, where c is the concentration of compound in mol/cm^3. The degree of reversibility for both electron transfers is indicated by the relationship i_{pa}/i_{pc}, which is close to 1, the value that describes reversible systems (Table 3).[16b] The values of $\Delta E_p = (E_{pa} - E_{pc})$ also approach the theoretical value of 60 mV reported for one-electron, reversible systems. The E_{pcI} values (Table 3) for the first one-electron transfer, corresponding to the formation of the radical-anion (eq 4), are in the potential range of −1096 to −1223 mV. For the second one-electron transfer, the E_{pcII} values leading to the formation of the corresponding dianion (eq 5) fall within the range of −1594 to −1731 mV (Table 3). The variation in peak potential indicates the influence of the substituent on the redox properties of APZm.

Table 3. Electrochemical Parameters[a] of the (2-(1,5-Dimethyl-4-hexenyl)-3-hydroxy-5-methyl-1,4-benzoquinone and Its 6-[4′-(R_2-phenyl)amine] and 3-Methoxy-6-[4′-(R_2-phenyl)amine] Derivatives

		$i_{pc}v^{-1/2}c^{-1}$ ($AV^{-1/2}$ $s^{1/2}$ mol^{-1} cm^3)		i_{pa}/i_{pc}		ΔE_p (mV)		E_{pc} (mV)	
compd	σ_p[b]	wave I or I′	wave II or II′	wave I or I′	wave II or II′	wave I or I′	wave II or II′	wave I or I′	wave II or II′
PZm		34.1	25.4	1.03	1.06	68	79	−1113	−1635
p-MeOAPZm	−0.27	44.3	31.6	1.16	1.05	60	65	−1223	−1731
p-MeAPZm	−0.17	51.6	45.6	0.84	0.94	69	73	−1216	−1762
APZm	0.00	62.5	48.9	0.81	1.01	70	63	−1197	−1714
p-BrAPZm	0.23	31.3	16.7	0.80	1.18	69	72	−1165	−1646
p-CNAPZm	0.66	48.3	35.6	1.02	1.15	76	62	−1096	−1594
PZ		48.0	[c]	0.48	1.12	315	71	−926	−1720 (−1654)[d]
p-MeOAPZ	−0.27	39.9[e]	[c]	0.21	1.09	494	113	−1096	−1900 (−1840)[d]
p-MeAPZ	−0.17	[c]	[c]	0.25	1.07	437	101	−1062	−1910 (−1891)[d]
APZ	0.00	27.8[e]	[c]	0.44	0.86	478	75	−1015	−1808 (−1823)[d]
p-BrAPZ	0.23	33.1[e]	[c]	0.27	1.20	449	146	−1011	−1882 (−1777)[d]
p-CNAPZ	0.66	[c]	[c]	0.61	0.23	317	162	−925	−1745 (−1679)[d]

[a] Measured by cyclic voltammetry (mV vs Fc/Fc^+), 0.1 M Et_4NBF_4/acetonitrile with glassy carbon electrode (7 mm^2). [b] The standard Hammett values were taken from ref 32. [c] The values varied with the scan rate potential. [d] E_{pc} values obtained after addition of $Me_4N^+C_6H_5O^-$ to corresponding APZs are given in parentheses. [e] These values correspond to the independent behavior of voltamperommetric function with respect to the scan rate potential.

The ratio of current function of the second peak to the first reduction peak was lower than expected for a simple EE reaction. This suggests a reaction after the first reduction step, e.g., the disproportionation of the radical anion ($APZ^{\bullet -}$) as shown in eq 6. Such a phenomenon has been observed in other two-step electrochemical processes as described theoretically by Lehman and Evans.[35,36] Equation 6 associates a very small equilibrium constant (K) and also a very small forward constant kinetic rate (k_f), especially in aprotic conditions where $APZm^{2-}$ is present.[35,36] The voltammetric behavior presents no kinetic complications, however, the current function is sensitive to this phenomenon.[35, 36]

$$2APZ^{\bullet -} \underset{k_b}{\overset{k_f}{\rightleftharpoons}} APZm + APZm^{2-} \quad K = \frac{k_b}{k_f} \qquad (6)$$

Electrochemical Behavior of APZ Derivatives. Figure 5b shows the typical electrochemical behavior of APZ. The same behavior was observed for all its derivatives within the sweep potential range of 100−1000 mVs^{-1}. Voltammograms for all the compounds studied are very different from the typical behavior observed for quinone reduction in aprotic media (Figure 5a)[16] indicating that an additional effect must be operating on the electrode process in the APZ derivatives. Since the only structural difference between the compounds is the replacement of the −OMe group with an −OH group at the C_3 position (Figure 1, Table 1), the proton in the −OH group must be responsible for the altered electrochemical behavior. It is important to recall that quinones containing phenolic groups (i.e., 1,8-dihydroxyanthraquinone[19] and 1-hydroxy-9,10-anthraquinone[20]) maintain the typical electrochemical behavior of quinones despite intramolecular hydrogen bonding. Thus, the APZ series difference in electrochemical behavior is due to elevated acidity of the −OH group in these molecules since the −OH group is located on the quinone ring**.** The electrochemical reactions associated with each voltammetric peak in the APZ cases, certainly differ from those associated with the voltammetric peaks obtained for APZm. Nevertheless, we report the voltammetric parameters for the APZ series as peak I′ and peak II′ in Table 3. The results show that the value of the current function $i_{pc}v^{-1/2}c^{-1}$ is not constant with the scan rate potential for all APZs. Moreover, the values obtained for most of the APZs were less than for the corresponding APZms (Table 3). As the size and shape of the APZm and APZ derivatives are very similar, the decrease in current function can not be attributed to a change in diffusion coefficient. The ΔE_p values ($E_{pa\prime} - E_{pc\prime}$) for peak I'_c (Table 3) are in the range of 315−494 mV, much higher than the value of 60 mV reported for the simple, one-electron systems.[16b] This large ΔE_p value merely indicates irreversibility in the system due to kinetics or coupled chemical reactions. The ratio of i_{pa}/i_{pc}, for peak I'_c confirms the presence of chemical reactions coupled to electron-transfer and, accordingly, the values of the half-wave potential could not be calculated. Only the cathodic peak potentials for these compounds (E_{pc}), obtained at 100 mVs^{-1} for both waves, are described in Table 3.

Electrochemical behaviors similar to that displayed by APZs (Figure 5b and Table 3) have been observed in electrochemical reduction of quinones in electrolytic media containing proton donors[18] as well as in quinones with acidic protons in their structure (HQ).[17] For the latter type of molecules that have functional groups with acidic characteristics, such as the −OH group at position C_3 of the perezone, reduction of the quinone (HQ) has been described as occurring via the reactions shown in eqs 7−10.

Since in these experiments no donor proton was present, the acidic hydrogen of the −OH in the APZ molecule (HQ) acts as an inner proton donor in a typical self-protonation reaction.

$$HQ + 1e^- \rightleftarrows HQ^{\bullet -} \qquad (7)$$

$$HQ^{\bullet -} + HQ \rightleftarrows HQH^{\bullet} + Q^- \qquad (8)$$

$$HQH^{\bullet} + 1e^- \rightleftarrows HQH^- \qquad (9)$$

$$HQH^- + HQ \rightleftarrows HQH_2 + Q^- \qquad (10)$$

$$HQ + {}^2/_3\, e^- \rightleftarrows {}^1/_3\, HQH_2 + {}^2/_3\, Q^- \qquad (11)$$

(35) Evans, D. H.; Lehmann, M. W. *Acta Chim. Scand.* **1999**, *53*, 765−774.

(36) Lehmann, M. W.; Evans, D. H. *Anal. Chem.* **1999**, *71*, 1947−1950

According to reactions 7−10, we conclude that the first reduction wave (I'_c) observed in the cyclic voltammograms of the APZ (HQ) derivatives (Figure 5b) corresponds to the overall reaction 11 in which the quinone is reduced through 2/3 of an electron to produce the corresponding hydroquinone HQH_2 and the perezonate Q^-. In these reactions, part of HQ is used for the redox reactions (eqs 7 and 9) and another part for the protonation reactions (eqs 8 and 10). This effect diminishes the quantity of quinone transformed to hydroquinone. The decrease in current function value (Table 3, peak I'_c) and reduction current observed for the first cathodic wave of the APZs compared to that corresponding to the APZms (Figure 5a,b) substantiates these effects. The cathodic peak potential for the first wave (peak I'_c) from the APZs is less negative than the corresponding value from the APZms (peak I_c), as seen in Table 3 (i.e., $E_{pcI'}$ for APZ is 104 mV higher than E_{pcI} for APZm). A lower charge density occurs in the APZs system due to formation of a hydrogen bridge between the −OH group and the adjacent carbonyl group $C_4{-}O_4$ (Figure 4a) stabilizing the anion-radical of the APZ. This effect is also observed for α-phenolic quinones, however, the direct proton transfer to the anion-radical (equation 8) is absent. APZs thus have less negative reduction potentials than the corresponding APZms.

Previous studies on this type of molecules[22,25] only investigated the electroreduction process that occurred in the first wave. In a recent work[37] and in the present study, the process corresponding to the second wave (II'_c), was evaluated as well.

Intermediates formed in the sequence of reactions 7−10 suggest that, at the negative potentials of the second wave (−1720 to −1910 mV), the only species that can exist on the electrode interface is perezonate (Q^-) formed in the self-protonation reactions (eqs 8 and 10). We therefore proposed that the second reduction process observed in the APZs corresponds to reduction of this intermediate.

$$Q^- + 1e^- \rightleftarrows Q^{\bullet 2-} \qquad (12)$$

To test if the second reduction process of the APZ series (Figure 5b) corresponded to reaction 12, a strong base was used to generate perezonate Q^- in the solution. Pilaj and Murray also added a strong base to the hydroxyquinone solution to analyze the electrochemical behavior corresponding to the conjugated base of this quinone[20] In our experiments, cyclic voltammetry was carried out in electrolytic media containing 2 mM of tetramethylammonium phenolate ($Me_4N^+C_6H_5O^-$) (Figure 6b). Under these conditions, the first wave (peak I'_c) corresponding to the reduction of APZ, disappeared and the second wave became broad and irreversible. Regardless of the quantity of $Me_4N^+C_6H_5O^-$ added to the solution, a small quantity of APZ remained in solution, as detected by a small prepeak observed in Figure 6b. A previous study showed that the cathodic peak associated with APZ reduction presents a negative shift and a decrease of its associated current when the phenolate concentration was increased.[38] This behavior provides further compelling evidence that

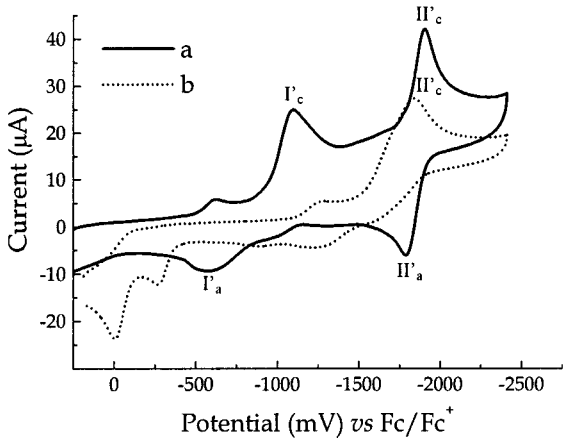

Figure 6. Typical cyclic voltammograms for 1 mM *p*-MeOAPZ in 0.1 M Et_4BNF_4/acetonitrile obtained with a glassy carbon electrode (7 mm^2), at 100 mVs^{-1} scan rate: (a) in the absence of $Me_4N^+C_6H_5O^-$ and (b) in the presence of 2 mM $Me_4N^+C_6H_5O^-$.

$Me_4N^+C_6H_5O^-$ is a sufficiently strong base to deprotonate the −OH group on the APZ (HQ) derivatives (eq 13) and generate perezonate (Q^-).

$$HQ + C_6H_5O^- \rightleftarrows C_6H_5OH + Q^- \qquad (13)$$

Perezonate is responsible for the cathodic peak (II'_c) observed at potentials in the range of −1654 to −1891 mV (Table 3). Unlike the behavior observed in aprotic medium (Figure 6a), in the presence of $Me_4N^+C_6H_5O^-$, the perezonate reduction peak is an irreversible process (Figure 6b). In the voltammograms (Figure 6a) of the APZ series, sometimes a small peak precedes peak I'_c, probably due to an adsorption process. The current associated with this pre-peak shows more significant variation with the scan rate than that of peak I'_c confirming the adsorption processes involved in the pre-peak. Analysis of the reversible behavior of the perezonate peak and the adsorption process mentioned above require a more detailed electrochemical study which is beyond the scope of this work.

Substitution Effects. The cyclic voltammogram of PZ was similar to that of APZ, both complicated by the presence of chemical reactions caused by self-protonation. The aniline substituent at the C_6 position in APZ made the electroreduction process more difficult compared with that of PZ (Table 3) since the electron-donor ability of the nitrogen atom increases the electronic density in the quinone system. This effect also caused the hydrogen of the hydroxyl group in APZ to be less acidic than in PZ.

The introduction of 4′-para substituents on the aniline ring in APZm produced significant negative and positive shifts in the peak potential associated with the first reduction process depending on the electronic effect of the substituent. As observed in similar systems,[24] even when the substituent is not directly conjugated with the quinone group, the substitution effect of the aniline system on electrochemical reduction of the quinone is evident. Methoxy and methyl electron-donor groups on the APZm made reduction of the quinone more difficult than for APZm (Table 3), while with the electron-accepting groups the opposite effect was observed.

In the APZ series, the substituents also displayed electronic effects according to their σ_p Hammett constants

(37) Ferraz, P. A. L.; de Abreu, F. C.; Pinto, A. V.; Glezer, V.; Tonholo, J.; Goulart, M. O. F. *J. Electroanal. Chem.* **2001**, *507*, 275−286.

(38) J. A. Bautista-Martínez, M. Sc. Thesis, UNAM Facultad de Química, Mexico, 2000.

despite the fact that the electrochemical reaction associated at the first reduction process is different for APZ and APZm (see reactions 11 and 4, respectively). The magnitude of this effect was less for APZm than for APZ.

Reduction of perezonate (wave II′$_c$, Figure 6b) formed during the reaction of APZs and $Me_4N^+C_6H_5O^-$ also was influenced by the substituents. Electron-donor substituents caused $E_{pcII'}$ values (shown in parentheses in Table 3) to shift toward more negative potentials than the corresponding unsubstituted APZ. The opposite effect was observed for the electron-accepting substituents.

Hammett−Zuman Context. For a better understanding of the electroreduction mechanism, the electronic effects of different substituents R_2 (Table 1) in the E_{pc} potentials were studied using the Hammett−Zuman equation (eq 14)[39] and Hammett σ_p constants.[32]

$$\Delta E_{pc} = E^R_{pc} - E^H_{pc} = \rho_\pi \sigma_p \qquad (14)$$

Where E^H_{pc} is the reduction potential of the unsubstituted parent compound, E^R_{pc} is the reduction potential of the substituted compound and ρ_π is the reaction constant.

The two reaction series, APZs (HQ) and APZms, were evaluated. The corresponding relationships for the transformation of HQ to HQH_2 (eq 11) in APZs and of APZm to $APZm^{\bullet -}$ (eq 4) in the APZms in aprotic medium are described in the following equations (eqs 15 and 16, respectively):

$$\Delta E_{pc}\,(\mathrm{mV})_{APZ} = 171\sigma_p - 0.0218 \quad (n = 5,\ r = 0.95) \qquad (15)$$

$$\Delta E_{pc}\,(\mathrm{mV})_{APZm} = 147\sigma_p - 0.0005\ (n = 5,\ r = 0.98) \qquad (16)$$

In the APZs system, the relationship between the values of the $E_{pcI'}$ and the ρ_π-constant characterizes not only the stage of heterogeneous electron-transfer but also the subsequent homogeneous chemical reaction connected with the radical-anion protonation (eqs 7−10). However, in the case of APZms, reversibility of the first stage mentioned above precludes subsequent chemical reactions (eq 4).

Sensitivity of the reaction to the electronic effect of the substituents, characterized by positive values of the ρ_π-constant (the slope in eqs 15 and 16), indicates that there is an important substituent effect for both series. The reaction is facilitated by low electronic density on the electro active group, and the electron-accepting ability of these APZms and APZs follows a linear relationship to the electronic perturbation of the substituents. However, the APZs are more susceptible to the electron-donor substituent effect than the APZms. As mentioned above, the −OH in the APZs polarizes the carbonyl C_4-O_4 (Figure 4) causing the substituent, R_2, to have greater electron-donor and electron-accepting properties than the APZm series.

A correlation between the reduction potentials and Hammett's σ_p-constants has also been established in the case of the second electron transfer in APZms. The value of the ρ_π-constant (eq 17) indicates that the reduction of $APZm^{\bullet -}$ to $APZm^{2-}$ is also sensitive to the substituents' effects.

$$\Delta E_{pc}\,(\mathrm{mV})_{APZ} = 156\sigma_p - 0.003 \quad (n = 5,\ r = 0.84) \qquad (17)$$

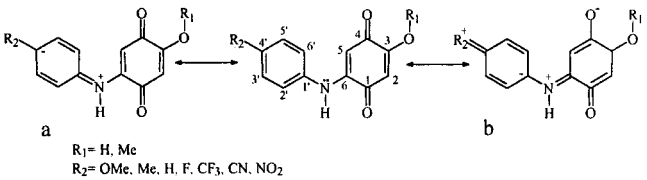

Figure 7. Dominant hybrids of ABQs and ABQms (model compounds for APZs and APZms) according to the electronic properties of the substituents: (a) effect of the electron-accepting groups; (b) effect of the electron-donor groups at the aniline moiety.

A relationship between ΔE_p for quinones with and without −OH in their structures has been described previously.[21,36]

The reduction of anilineperezonates (eq 12) was evaluated by analyzing the cathodic peaks (peak II′$_c$, $E_{pcAPZ-C_6H_5O^-}$) obtained in the cyclic voltammogram of APZs (HQ) in the presence of $Me_4N^+C_6H_5O^-$ (eq 18). The ρ_π value illustrates that $Q^{\bullet 2-}$ is highly unstable due to the increased charge density in the system, and the dianion-radical formed in the electroreduction process of perezonate (eq 12) is very sensitive to the effect of the substituents. The electron-accepting substituents thereby help to stabilize the charge excess in the system.[21,36]

$$\Delta E_{pc}\,(\mathrm{mV})_{APZ-C_6H_5O^-} = 204\sigma_p - 0.0026 \qquad (n = 5,\ r = 0.90) \qquad (18)$$

Theoretical Calculations. To interpret our experimental observations, we performed a full geometry optimization of model *p*-benzoquinones, substituted by a *p*-substituted-aniline group at position 6 and by hydroxy or methoxy groups at position 3, ABQ and ABQm, respectively (Figure 7). Models are useful here due to the large number of conformers associated with the rotation of the side chain. Recently, we found evidence of a conformer where the isolated double bond interacts with the quinone ring. Computational requirements increase rapidly with respect to the number of electrons taken into account. A full explanation of the model design is discussed below. The studies were performed within the framework of density functional theory[40] with the B3LYP hybrid functional, using a double ξ split valence basis set as implemented in Gaussian 94 (G94) programs.[41] Relevant geometric data are included in Table S1 of the Supporting Information. Table S2 (Supporting Information) shows the Wiberg bond indexes (WBI), calculated with the natural bond orbital program (NBO)[42] at a B3LYP/6-31G(d,p) level of theory, as well as the densities of the relevant critical points (ρ) and the Laplacians ($\nabla^2\rho$)

(39) Zuman, P. *Collect. Czech. Chem. Comun.* **1962**, *27*, 2035−2057.

(40) Malkin, V. G.; Malkina, O. L.; Eriksson, L. A.; Salahub, D. R. In *Modern Density Functional Theory. A tool for Chemistry*; Seminario, J. M., Politzer, P., Eds.; Elsevier: Amsterdam, 1995.

(41) Frisch, M. J.; Trucks, G. W.; Schlegel, H. B.; Gill, P. M. W.; Johnson, B. G.; Robb, M. A.; Cheeseman, J. R.; Keith, T.; Peterson, G. A.; Montgomery, J. A.; Raghavachar, K.; Al-Laham, M. A.; Zakrzewski, V. G.; Ortiz, J. V.; Foresman, J. B.; Cioslowski, J.; Stefanov, B. B.; Nanayakkara, A.; Challacombe, M.; Peng, C. Y.; Ayala, P. Y.; Chen, W.; Wong, M. W.; Andres, J. L.; Replogle, E. S.; Gomper, R.; Martin, R. L.; Fox, D. J.; Binkley, J. S.; Defrees, D. J.; Baker, J.; Stewart, J. P.; Head-Gordon, M.; Gonzalez, C.; Pople, A. *Gaussian 94, Revision E2*; Gaussian, Inc.: Pittsburgh, PA, 1995.

(42) Glendening, E. D.; Badenhoop, J. K.; Reed, A. E.; Carpenter, J. E.; Weinhold, F. *NBO 3.1*; Theoretical Chemistry Institute, University of Wisconsin: Madison, WI, 1994.

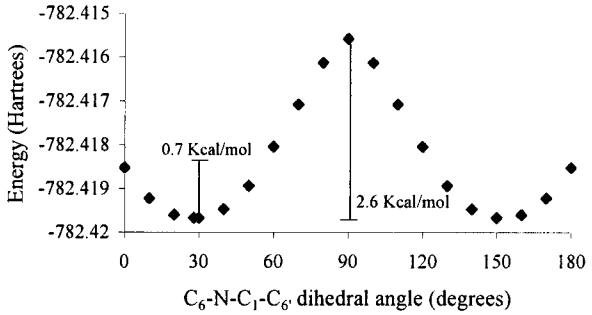

Figure 8. Dependence between the $C_6-N-C_1-C_{6'}$ dihedral angle and energy of the ABQm molecule.

and ellipticities (ϵ) determined using the AIM program.[43] Table S3 includes the natural charges and Table S4 (Supporting Information) the total and HOMO−LUMO energies. We determined the critical bond point densities of the compounds studied here according to the topological theory of atoms in molecules.[44]

The ABQ derivatives (Figure 7, $R_1 = H$) are flat, and analysis of the normal vibrational modes establishes correspondence to minimal points on the potential surface since all the frequencies are positive. We thus expect that the methoxylated derivatives are also flat as they experience the stabilizing effect provided by complete conjugation of the system. However, total planarity results in proximity of the hydrogen atoms at positions 5 and 6' to produce steric repulsion. Complete optimization of the geometry of the ABQm from flat structures permits isolation of stationary points whose geometries are described in Table S1 (Supporting Information). Analysis of the normal modes of vibration, however, establishes that the flat arrangements correspond to transition states associated with rotation around the $C_1'-N$ bond (Figure 7). We evaluated the effect of rotation of this bond on the energy of the system. For $R_2 = H$ (ABQ), the value of the energy was determined every 10 degrees of the dihedral angle $C_6-N-C_1-C_{6'}$ obtaining the profile shown in Figure 8. At this potential, two maximal points, one corresponding to the flat molecule located at 0.7 kcal/mol with respect to the minimal located at 27.9° and the other located at 90°, are observed. The absolute minimum corresponds to the point where the dihedral angle is 27.9°. The geometric properties of this compound are described in table S1. As expected, at the latter point (90°) the conjugation is broken reinforcing the importance of the hydrogen bridge as a stabilizing contribution present on the ABQ series and absent on ABQm. The final geometry is the result of a fine balance between the hydrogen bridge and the repulsion between hydrogen atoms at positions 5 and 6′ (Figure 7). A difference of only 0.7 kcal/mol suggests a molecule with free rotation at that region and, thus, its description by only one group of coordinates is impossible and the molecule corresponds to the type denominated as fluxional. The planar structure of ABQ is very different from the structure of the parent APZ, in which, according to the X-ray structure shown in Figure S1 and tables S4-S8 (Supporting Information), the aniline ring is rotated and the dihedral angles are: $C_{1'}-N-C_6-C_5$ (31.5°) and $C_{6'}-C_{1'}-N-C_6$ (42°) with respect to the quinone plane. This rotation is due to the greater steric repulsion of the methyl group than of the hydrogen atom located at C_5, and methyl group dominance over the hydrogen bond stabilizing contribution.

Evaluation of the APZ crystal revealed several important structural characteristics. The bond distance is greater for C_4-O_4 than for C_1-O_1 as supported by theoretical calculations at the B3LYP/6-31G(d,p) level of theory for the model *p*-benzoquinones used in this study (see below). The quinone ring is slightly distorted from planarity with the $C_5-C_6-C_1-C_2$ dihedral angle equal to 5.5°. This distortion is possibly the result of steric strain. Two different intramolecular hydrogen bonds were determined. The $C_4-O_4\cdots H-O_3$ bond is stronger than $C_1-O_1\cdots H-N$, as expected, and bond distances are 2.079 and 2.224 Å, respectively. The $O_4\cdots H(O_3)$ bond favors electron donation from the aniline group and explains the bond length pattern. The nitrogen atom is pyramidalized with the angle between the $H-N-C_6$ and $C_{1'}-C_6-H$ planes equal to 30.4°. In planar nitrogen, this angle would be 0°. The bond length pattern in the $N-C_6-C_5-C_4-O_4$ segment supports the existence of the resonance hybrids suggested in Figure 7.

The molecular geometry is attributable to the equilibrium between the steric destabilizing and the stabilizing electronic delocalization contributions. Since the electronic effects are maximized in a planar system, in our molecular ABQ models we substituted the methyl group with a hydrogen atom allowing a highly conjugated, planar molecular frame. For the ABQms, we analyzed planar structures located at only 0.7 kcal/mol with respect the minimum in the molecule in order to maintain constant the full electronic delocalization. Energy of 0.7 kcal/mol is less than that of the zero point energy correction. Two different hydrogen bridges are observed in the model derivatives of APZs (Figure 9). The $O_4-H(O)$ bond distance is less than that of $O_1-H(N)$. The Wiberg bond index and the electronic density at critical bond point (Table S2, Supporting Information) are greater for the hydrogen bridge formed by the oxygen than by the nitrogen atom. In both cases, the Laplacians are positive, indicating the high ionic character of the interaction. The hydrogen bridge $O_4\cdots H(O)$ is sensitive to the effect of the substituents. Thus, the $O_4-H(O)$ distance of the ABQ series increases gradually from 1.880 Å when $R_2 = -OMe$ to 1.914 when $R_2 = -CN$. For the nitro group, the distance increases only to 1.915 Å. The N−H bridge does not show a definite trend in bond distance or in electronic density of the critical bond point (Tables S1 and S2). The bonding strength of O−H, therefore, is decreased by electron-accepting groups and increased by the electron-donor groups. This is evidence of the participation of the resonant forms shown in Figure 7.

Theoretical calculations establish that the nitrogen atom joining the quinone to the phenyl-substituted group hinders direct conjugation between these groups, interacting with one or the other, depending on the substituent. Electron-donor groups favor interaction with the quinoid ring (Figure 7b), while electron-accepting groups favor interaction with the aromatic ring (Figure 7a). The pattern of bond lengths in the segment $C_{1'}-N-C_6-C_5-C_4-O_4$ shows that for the hydroxylated derivatives, as the attractant character of the substituent increases, the

(43) Biegler-Koenig, F. W.; Bader, R. F. W.; Tang, T. H. *J. Comput. Chem.* **1982**, *2*, 317−328.

(44) (a) Bader, R. F. W. *Atoms in Molecules—A Quantum Theory*; Clarendon Press. Oxford, 1990. (b) Bader, R. F. W. *Acc. Chem. Res.* **1985**, *18*, 9−15. (c) Bader, R. F. W. *Chem. Rev.* **1991**, *91*, 893−928.

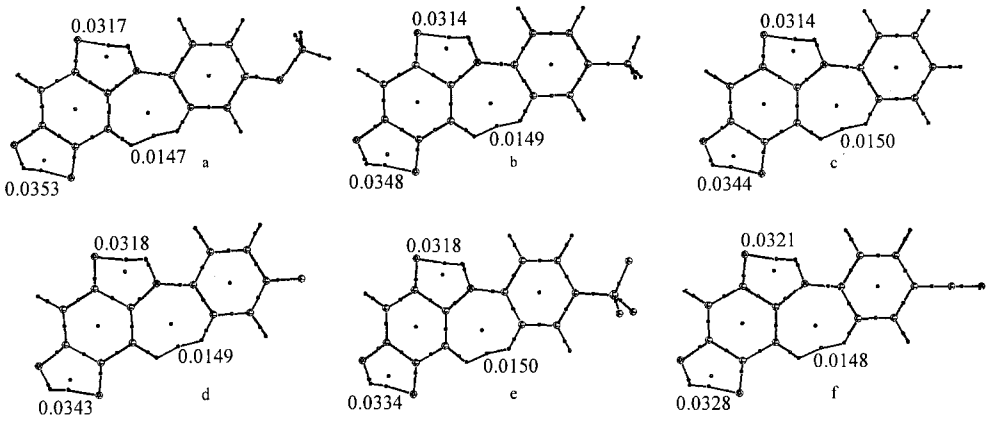

Figure 9. Bond and ring critical points in the density of 6-[4′-(R_2-phenyl)amine]-3-hydroxy-1,4-benzoquinones. R_2= −OMe (a), $-CH_3$ (b), −H (c), −F (d), $-CF_3$ (e), −CN (f). Values correspond to the density of bond critical points.

distances $N-C_{1'}$, C_5-C_6, and C_4-O_4 tend to decrease, while the C_6-N and C_5-C_4 distances tend to increase. In contrast, the segment $O_3-C_3-C_2-C_1-O_1$ does not change with substituent variation. The $C_6-N-C_{1'}$ angle remains constant regardless of the nature of the substituent since the $H_5-H_{6'}$ repulsion dominates. In the case of the $-NO_2$ group, the $H_5-H_{6'}$ repulsion increases noticeably due to shortening of the $N-C_{1'}$ bond, justifying the loss of molecular planarity.

Insensitivity of the segment $O_3-C_3-C_2-C_1-O_1$ to substituent effects is unexpected since the electron-donor groups that favor participation of the nitrogen atoms in the delocalization of the quinone should increase the interaction of the O_3 proton with O_4, favoring participation of the resonant form (*b*) shown in Figure 4. We conclude that for an isolated molecule in the vapor phase at 0 K, there is no participation of the resonating form 4b, since the average O_1-C_1 distance is 1.233 Å and this distance is insensitive to the effect of the substituents. In comparison, the O_4-C_4 distance varies from 1.242 to 1.237 Å when the −OMe group is changed for the $-NO_2$ group.

The C−C═O valence angles of the two carbonyl groups on the quinone tend to be approximately 6° smaller on the side forming the hydrogen bond than on the side where no such bonds form. The C_3-O_3 bond displays similar behavior. In contrast, on the methylated derivatives the O_4-C_4 distance is notably less than the C_1-O_1 distance. This may be due to the absence of the hydrogen bridge that produces polarization of the carbonyl group and facilitates the resonant form (a) in Figure 4. In addition, the patterns of bonding lengths for the $C_{1'}-N-C_6-C_5-C_4-O_4$ and $O_3-C_3-C_2-C_1-O_1$ segments decrease in intensity for the same para substituent between the −OH and −OMe series.

Table S9 (Supporting Information) shows the effect of rotation around the dihedral angle $C_6-N_2-C_{1'}$-$C_{6'}$ on the density of the relevant critical points of ABQm. The density of the molecule's critical points on the minimal energy conformation (27.94°) does not change substantially with respect to the flat structure and does not change the previous arguments. In addition, as the dihedral angle of interest increases, the C_6-N bond becomes stronger because the nitrogen decreases its delocalization effect on the aromatic ring and thus, increases the possibility of interacting with the quinone. The $N-C_{1'}$ bond shows the opposite trend when its angle reaches 90°, conjugation decreases notably. Variation of electronic delocalization is not influenced by the total molecular energy and the electronic density on the conjugated system tends to increase for the C_6-C_5, C_5-C_4 bonds. Electronic density is practically constant for the C_4-O bond while on the C_4-C_3, C_3-C_2, C_1-C_2 bonds, it shows a decrease of ρ. This can not be explained in terms of electronic delocalization (π) but rather in terms of the inductive effect and stresses. To compare the ABQ with ABQm series for determining the effect of the hydrogen bridge, these bonds need to be kept flat.

Analysis of the Wiberg bond indexes and the electronic density of the critical points and their Laplacians (Table S2, Supporting Information) leads us to hypothesize that the electronic delocalization is greater in the hydroxylated than in the methoxylated derivatives. The $C_{1'}-N-C_6-C_5-C_4-O_4$ segment produces a pattern of bond order and electronic density that agrees with the resonant forms described in Figure 7. In addition, the nitrogen atom of the aniline interacts with the aromatic ring when it is substituted with electron-accepting groups and with the quinoid ring when the substituents are electron-donors.

Besides the hydrogen bridges already described, the study of molecular topology through the bond and ring critical points revealed an unexpected $H_5-H_{6'}$ bonding path (Figure 9). This unexpected critical point corresponds to an interaction line between the attractors of steric origin and corresponds to the dihydrogen interaction (so-called dihydrogen-bridge).[45] Such interactions have been described by Cioslowski[46] and the interaction distance ($H_5-H_{6'}$) found for the compounds studied here agrees with those previously reported.[24] The interaction is observed in the model molecules used in those studies because it considered a proton at the C_5 position, however APZs and APZms have a methyl group in that position and thus, the $H_5-H_{6'}$ interaction does not exist.

The Laplacians $\nabla^2\rho$ are very sensitive to electronic delocalization. Behavior of the carbonyl group in the compounds studied allowed us to efficiently differentiate between the two quinone carbonyl groups. For the −OH series, the Laplacians of the critical points of the C−O bonds indicate an increased ionic character (positive Laplacians values, Table S2, Supporting Information)

(45) Alkorta, I.; Rozas, I.; Elguero, J. *Chem. Soc. Rev.* **1998**, *27*, 163−170.

(46) (a) Cioslowski, J.; Mixon, S. T.; Edwards, W. D. *J. Am. Chem. Soc.* **1991**, *113*, 1083−1085. (b) Cioslowski, J.; Mixon, S. T. *J. Am. Chem. Soc.* **1992**, *114*, 4382−4387.

Table 4. Energy of the Frontier Orbitals and Their Neighbors for 6-[4′-(R_2-phenyl)amine]-3-hydroxy-1,4-benzoquinones (ABQs) and 6-[4′-(R_2-phenyl)amine]-3-methoxy-1,4-benzoquinones (ABQms) (Energy in Hartrees)

compd	$E_{HOMO} - 1$	E_{HOMO}	E_{LUMO}	$E_{LUMO} + 1$	η	E_{total}
p-MeOABQ	−0.24949	−0.20773	−0.10642	−0.02086	0.05066	−857.65195
p-MeABQ	−0.2556	−0.21656	−0.10933	−0.01916	0.05362	−782.44815
ABQ	−0.25908	−0.22158	−0.11165	−0.01945	0.05497	−743.12730
p-FABQ	−0.26027	−0.22241	−0.11377	−0.03081	0.05432	−842.35738
p- CF_3ABQ	−0.26798	−0.23365	−0.12086	−0.03941	0.05640	−1080.16221
p-CNABQ	−0.27123	−0.23793	−0.12645	−0.05785	0.05574	−835.36797
p- NO_2ABQ	−0.27442	−0.24324	−0.12867	−0.09241	0.05729	−794.62737
p-MeOABQm	−0.24673	−0.19756	−0.09898	−0.01293	0.04929	−896.94255
p-MeABQm	−0.24967	−0.20610	−0.10148	−0.01152	0.05231	−821.73910
ABQm	−0.25189	−0.21104	−0.10349	−0.01225	0.05375	−782.41852
p-FABQm	−0.25405	−0.21195	−0.10564	−0.02274	0.05316	−881.64866
p- CF_3ABQm	−0.26105	−0.22392	−0.11243	−0.03243	0.05575	−1119.45424
p-CNABQm	−0.26623	−0.22848	−0.11782	−0.05101	0.05560	−874.66038
p- NO_2ABQm	−0.26764	−0.23416	−0.12024	−0.08584	0.05696	−956.91991

with the C_1-O_1 group being more electrophilic than C_4-O_4 (natural charges in Table S3, Supporting Information). For isolated molecules in gas phase, C_4 is more electrophilic in the −OMe than in −OH series, as shown in ^{13}C NMR observations. For the ABQ series, on the other hand, the hydrogen bridge $O_1-H(N)$ polarizes the C_1-O_1 group, but the donating oxygen at C_3 makes the carbonyl group at C_4 more susceptible to the addition of an electron, protecting C_1 from electronic addition and increasing the strength of the hydrogen bridge. The opposite is observed for the methoxy series, where the donor capabilities of the oxygen atom at C_3 are diminished. The Laplacians of the critical points in both cases support participation of the resonant forms shown in Figure 7.

Table 4 includes the energies of the frontier molecular orbitals as well as the absolute hardness (η), defined as $(E_{LUMO} - E_{HOMO})/2$. For all compounds, the NBO analysis established that the HOMO orbital corresponds to the lone pair of one of the heteroatoms (mainly of the substituents on the aromatic ring) and the LUMO corresponds to the Rydberg orbital of sp type located at C_4. Interestingly, the LUMO at C_4 permits better interaction with the nitrogen lone pair making the charge-transfer associated with this interaction possible. Natural charges (Table S3, Supporting Information) show that C_1 is more positive than C_4, in agreement with an electronic transfer process activated by the N atom, and is more positive in the −OMe series than in the −OH series as shown in spectroscopic observations (see ^{13}C NMR chemical shifts). If the process is controlled by natural charge, the more sensitive carbonyl group would be C_1-O_1 and reduction would be easier in the methoxy than in the hydroxy series.[47] It is reasonable to locate the LUMO orbital at C_4 since it is closer in energy to the nitrogen lone pair allowing an efficient and dominant $n_N \rightarrow \pi^*$ stereoelectronic interaction.

A linear relationship occurs between the HOMO and LUMO orbital energies of these molecules and the experimental σ_p Hammett parameter (Table 5).

Absolute hardness (η) described in Table 4 is a reactivity index. For the same substituent in the phenyl ring, this value is greater for the ABQ with respect to the ABQm series and for nitro with respect to methoxy derivatives. These results contradict experimental observations since larger values of η imply more stable molecules, which is not the case for the molecules studied here. This demonstrates that overall hardness properties do not provide adequate reactivity indexes.[48]

Table 5. Parameters of the HOMO and LUMO Orbital Energies vs σ_p Hammett Constant Plots of 6-[4′-(R_2-phenyl)amine]-3-hydroxy-1,4-benzoquinones (ABQs) and 6-[4′-(R_2-phenyl)amine]-3-methoxy-1,4-benzoquinones (ABQms)

$E_x(\text{Hartrees}) = \rho_\pi \sigma + b$
with n molecules in the correlation and r correlation coefficient

E_x	series	ρ_π	b	n	r
E_{HOMO}	ABQms	−0.0305	−0.2090	7	0.98
E_{LUMO}	ABQms	−0.0194	−0.1041	7	0.98
E_{HOMO}	ABQs	−0.0293	−0.2195	7	0.97
E_{LUMO}	ABQs	−0.0203	−0.1121	7	0.98

Conclusions

We synthesized 13 novel derivatives of perezone that, with the exception of APZ and PZm, have not been previously reported (Table 1). PZ and APZs (HQ), which have an acidic hydrogen at the C_3 position, displayed very different electrochemical behavior than that of typical quinones. For the compounds containing acidic hydrogens, the cyclic voltammograms produced two waves. The first of these corresponded to the irreversible reduction from HQ to HQH_2, and the second to a one-electron transfer due to the reversible reduction from perezonate (Q^-) formed during the self-protonation reaction to $Q^{\bullet 2-}$. In basic media ($Me_4N^+C_6H_5O^-$), the cyclic voltammogram of APZs (HQ) showed only the wave corresponding to the Q^- to $Q^{\bullet 2-}$ reduction, confirming that the second wave in aprotic media is due to this reduction process. Following the methylation reaction of APZs, the presence of the two characteristic, one-electron charge-transfer waves was observed for APZm.

APZs and APZms are quinones-NH-substituted phenyls, in which the amine group located between the quinone and the substituted aryl groups interferes with the direct transmission of the substituent effect on the quinone system. We observed a linear variation of $1/\lambda_{max}$ for $n_N \rightarrow \pi^*$ and ^{13}C chemical shifts of the unsaturated carbons of perezone derivatives as a function of σ_p. This variation indicates a direct influence of the donor−acceptor properties of the substituent in the aniline ring on the electronic properties of the quinone ring. Our analysis of the effect of the substituents on the cathodic peak potentials (E_{pc}) demonstrated that this effect is

(47) Jensen, F. *Introduction to Computational Chemistry*; Wiley: New York, 1999; pp 347−348.

(48) (a) Perez, P.; Toro-Labbe, A.; Contreras, R. *J. Phys. Chem. A.* **2000**, *104*, 5882−5887. (b) Fuentealba, P.; Perez, P.; Contreras, R. *J. Chem. Phys.* **2000**, *113*. 2544−2551.

transmitted through the amine group. For the ρ_π constants in the first reduction wave, the APZs showed greater sensitivity to the effect of the substituent than for the same wave in the APZm series ($\rho_\pi = 171$ and $\rho_\pi = 147$, respectively). This observation is explained by the fact that in the APZs, the −OH group at C_3 polarizes the bond C_4-O_4 facilitating delocalization of the nitrogen lone pair into the quinone system. This substantiates our theoretical calculations that showed the pattern of bonding lengths of $C_{1'}-N-C_6-C_5-C_4-O_4$ and $O_3-C_3-C_2-C_1-O_1$ segments decreasing in intensity for the same *p*-substituent from the −OH to the −OMe series. According to Figure 7, displacement of the unshared nitrogen electrons mainly modifies the electronic density of the $C_{1'}-N-C_6-C_5-C_4-O_4$ segment and has less effect on the electronic density of the C_1-O_1 bond, as demonstrated by the Topological Theory of Atoms in Molecules indexes. For the APZms system, greater susceptibility of the second wave to the substitution effect ($\rho_\pi = 156$ mV) indicates that this wave corresponds to the reduction of carbonyl C_4-O_4. Natural charges show that C_1 is more positive than C_4; nevertheless, the LUMO orbital is located at C_4. Thus, the electrochemical transfer in which the quinone takes part is controlled by the natural charge distribution of the quinones rather than by their orbital energies, since the first wave belongs to the reduction of the carbonyl, C_1-O_1.

LUMO energy values calculated for the different APZs and APZms studied here predict that reduction facility will follow the order *p*-NO_2> *p*-CN> *p*-CF_3> *p*-F> *p*-H> *p*-Me> *p*-MeO. The reduction order agrees with the E_{pc} potentials (Table 3) obtained by cyclic voltammetry for the reduction of APZs and APZms in aprotic media. A good linear relationship between the E_{LUMO} and the corresponding E_{pcI} for APZm/APZm$^{\bullet-}$ reduction (eq 19) was observed.

$$E_{pcI}\,(\mathrm{mV})_{APZms} = -6714E_{LUMO}\,(\mathrm{Hartree}) - 1946 \quad (n = 4,\ r = 0.98) \quad (19)$$

The correlation was not so straightforward for the APZs (HQ) (eq 20) since in this system, in addition to the electron transfer, self-protonation reaction is taking place in the electrochemical process.

$$E_{pcI'}\,(\mathrm{mV})_{APZs} = -3422E_{LUMO}(\mathrm{Hartree}) - 1434 \quad (n = 4,\ r = 0.60) \quad (20)$$

Experimental Section

Synthesis. All reactions were carried out under inert nitrogen atmosphere. THF was distilled in an N_2 atmosphere prior to use over sodium-benzophenone ketyl and successively over $LiAlH_4$. Chromatographic purifications were carried out on silica gel columns(Merck, 230−400 mesh) at medium pressure using *n*-hexane−ethyl acetate (9:1) as eluent. PZ was isolated from *Perezia cuernavacana* roots as described by Walls,[27] as golden-yellow leaflets, mp 104−106 °C, $[\alpha]^{20}_D$ −17 (Et_2O). All other materials were purchased commercially. ^1H and ^{13}C NMR spectra (500 and 75 MHz, respectively) were recorded in $CDCl_3$ and used TMS as a reference. Signal multiplicity is described as follows: d, doublet; t, triplet; dq, doublet of quintets; ts, triplet of septets; m: multiplet. Molecular numbering is given in Table 1. Mass spectra and high-resolution mass spectra (HRMS) were performed by electron impact with beam energy of 70 eV. IR spectra were recorded in different media: directly as a film, in KBr pellets or in solution with $CHCl_3$. In the last case the solvent spectra was subtracted. Elemental analyses were performed by Galbraith Laboratories, Inc. Melting points are not corrected.

General Procedure (I) for the Preparation of Substituted 2-(1,5-Dimethyl-4-hexenyl)-3-hydroxy-5-methyl-6-[4′-(R_2-phenyl)amine]-1,4-benzoquinones (APZs). A 2.01 mmol portion of the substituted aniline (dissolved in 20 mL of anhydrous THF) was added dropwise via cannula with stirring to the solution of perezone (500 mg, 2.01 mmol) in 25 mL of anhydrous THF in a dry apparatus under N_2 atmosphere. A deep blue solution was obtained. The reaction mixture was refluxed for 12 h. After cooling, 10 mL of 2 N HCl was added, and the solvent was removed in a vacuum. The residue was dissolved in CH_2Cl_2 (50 mL), and the organic phase washed with water and brine and then dried. After the CH_2Cl_2 was evaporated, the residue was subjected to column chromatography (silica gel, *n*-hexane−ethyl acetate 9:1) yielding the desired product.

2-(1,5-Dimethyl-4-hexenyl)-3-hydroxy-5-methyl-6-[(4′-methoxyphenyl)amine]-1,4-benzoquinone (*p*-MeOAPZ). A 0.247 g portion of 4-methoxyaniline under general procedure I yielded 0.70 g (97%) of the product: mp 125−127 °C; IR ($CHCl_3$, cm^{-1}) 851, 929, 984, 1020, 1114, 1163; UV−vis (MeOH, nm) 543, 290, 257, 209; ^1H NMR ($CDCl_3$) δ 1.2 (d, 3H, $J = 7.0$ Hz, H_8), 1.57 (s, 3H, H_{14}), 1.55 (s, 3H, H_7), 1.6 (m, 1H, H_{10}), 1.65 (d, 3H, $J = 1$ Hz, H_{15}), 1.8 (m, 1H, H_{10}), 1.9 (m, 2H, H_{11}), 3.05 (dq, 1H, $J = 7.0$, 9.0 Hz, H_9), 3.93 (s, 3H, R_2), 5.05 (ts, 1H, $J = 1.5$, 7.0 Hz, H_{12}), 6.95 (d, 2H, $J = 9.0$ Hz, $H_{2',6'}$), 7.3 (s, 1H, OH), 7.6 (broad, 1H, NH), 7.97 (d, 2H, $J = 9.0$ Hz, $H_{3',5'}$); ^{13}C NMR ($CDCl_3$) δ 182.72 (C_1), 181.81 (C_4), 153.72 (C_3), 143.17 (C_6), 139.84 ($C_{4'}$), 131.33 ($C_{1'}$), 130.93 (C_{13}), 125.28 (C_2), 125.10 (C_{12}), 123.71 ($C_{3',5'}$), 118.5 (C_5), 112.68 ($C_{2',6'}$), 54.15 (R_2), 34.45 (C_{10}), 29.4 (C_9), 26.8 (C_{11}), 26.27 (C_{15}), 18.4 (C_8), 17.99 (C_{14}), 11.54 (C_7); MS *m*/*z* 369, 326, 312, 300, 298, 288, 287, 286, 272, 260, 258, 229, 131, 123, 91. Anal. Calcd for $C_{22}H_{27}O_4N$: C, 71.54, H, 7.31; N, 3.79. Found: C, 71.55; H, 7.19; N, 3.97.

2-(1,5-Dimethyl)-4-hexenyl)-3-hydroxy-6-[(4′-methylphenyl)amine]-1,4-benzoquinone (*p*-MeAPZ). According to general procedure I, 0.215 g (2 mmol) of *p*-toluidine yielded 0.639 g (90%) of the desired product: mp 117−118 °C; IR ($CHCl_3$, cm^{-1}) 928, 1020, 1058, 1092, 1112, 1175, 1293, 1313, 1337, 1378, 1401, 1456, 1494, 1516, 1585, 1618, 1641, 1701, 1717, 2011, 2045, 2859, 2928, 2961, 3050, 3313; UV−vis (MeOH, nm) 510, 315, 231; ^1H NMR ($CDCl_3$) δ 1.23 (d, 3H, $J = 7$ Hz, H_8), 1.51 (s, 3H, H_7), 1.58 (s, 3H, H_{14}), 1.6 (m, 1H, H_{10}), 1.66 (d, 3H, $J = 1.5$ Hz, H_{15}), 1.8 (m, 1H, H_{10}), 1.91 (m, 2H, H_{11}), 2.42 (s, 3H, R_2), 3.06 (dq, 1H, $J = 7$, 8.5 Hz, H_9), 5.1 (ts, 1H, $J = 1.5$, 7.0 Hz, H_{12}), 6.95 (d, 2H, $J = 8.0$ Hz, $H_{2',6'}$), 7.26 (d, 2H, $J = 8$ Hz, $H_{3',5'}$), 7.7 (s, 1H, OH), 8.1 (broad, 1H, NH); ^{13}C NMR ($CDCl_3$) δ 182.75 (C_1), 181.87 (C_4), 153.67 (C_3), 143.13 (C_6), 135.76 (C_{16}), 132.86 (C_{19}), 130.94 (C_{13}), 128.07 ($C_{3',5'}$), 125.82 (C_2), 125.04 (C_{12}), 121.58 ($C_{2',6'}$), 118.6 (C_5), 34.39 (C_{10}), 29.4 (C_9), 26.7 (C_{11}), 26.3 (C_{15}), 19.59 (R_2), 18.4 (C_8), 17.96 (C_{14}), 11.64 (C_7); MS *m*/*z* 353, 354, 272, 271, 270, 245, 244, 242, 198, 83. Anal. Calcd for $C_{22}H_{27}O_3N$; C, 74.78; H, 7.64; N, 396. Found: C, 74.56; H, 7.82; N, 3.97.

2-(1,5-Dimethyl-4-hexenyl)-3-hydroxy-5-methyl-6-phenylamine-1,4-benzoquinone (APZ). According to general procedure I, 0.187 g (2 mmol) of aniline yielded 0.644 g (95%) of the desired product: mp 132−133 °C; IR ($CHCl_3$, cm^{-1}) 1083, 1245, 1296, 1316, 1337, 1377, 1402, 1449, 1506, 1585, 1643, 2867, 2929, 2967, 3312; UV−vis (MeOH, nm) 535, 337, 260, 207; ^1H NMR ($CDCl_3$) δ 1.2 (d, 3H, $J = 7$ Hz, H_8), 1.5 (s, 6H, H_7, H_{14}) 1.6 (m, 1H, H_{10}), 1.69 (d, 3H, $J = 1.5$ Hz, H_{15}), 1.8 (m, 1H, H_{10}), 1.9 (m, 2H, H_{11}), 3.05 (dq, 1H, $J = 7$, 8.5 Hz, H_9), 4.75 (s, 1H, H_{16}), 5.1 (ts, 1H, $J = 1.5$, 7.0 Hz, H_{12}), 7.0 (d, 2H, $J = 7.5$ Hz, $H_{2',6'}$), 7.21 (t, 1H, R_2) 7.35 (d, 2H, $J = 7.5$ Hz, $H_{3',5'}$), 7.6 (broad, 1H, NH); ^{13}C NMR ($CDCl_3$) δ 182.8 (C_1), 181.97 (C_4), 153.6 (C_3), 143.06 (C_6), 138.51 ($C_{4'}$), 130.97 (C_{13}) 127.61 ($C_{3',5'}$), 126.74 (C_2), 124.95 (C_{12}), 121.26 ($C_{2',6'}$), 122.94 ($C_{1'}$), 118.76 (C_5), 34.27 (C_{10}), 29.7 (C_9), 26.52 (C_{11}), 26.35 (C_{15}), 18.4 (C_8), 17.9 (C_{14}), 11.82(C_7); MS *m*/*z* 339, 296, 282, 257, 230, 228, 180, 130, 109, 77, 69, 67, 55, 41. Anal. Calcd for $C_{21}H_{25}O_3N$; C, 74.33; H, 7.37; N, 4.12. Found: C, 74.10; H, 7.58; N, 4.02.

2-(1,5-Dimethyl-4-hexenyl)-3-hydroxy-5-methyl-6-[(4′-bromophenyl)amine]-1,4-benzoquinone (*p*-BrAPZ). A 0.346 g portion of 4-bromoaniline yielded 0.773 g (92%) of the desired product: mp 127−128 °C; IR (film, cm^{-1}) 816, 850, 933, 1011, 1071, 1092, 1172, 1247, 1286, 1306, 1335, 1377, 1396, 1453, 1502, 1581, 1603, 1641, 1700, 1743, 2858, 2875, 2927, 2966, 3316; UV−vis (MeOH, nm) 521, 345; ^{1}H NMR ($CDCl_3$) δ 1.21 (d, 3H, J = 7.0 Hz, H_8), 1.55 (s, 3H, H_{14}), 1.59 (s, 3H, H_7), 1.6 (m, 1H, H_{10}), 1.67 (d, 3H, J = 1.5 Hz, H_{15}), 1.87 (m, 1H, H_{10}), 1.95 (m, 2H, H_{11}), 3.05 (dq, 1H, J = 7.0, 8.5 Hz, H_9), 5.09 (ts, 1H, J = 1.5, 7.0 Hz, H_{12}), 6.95 (d, 2H, J = 8.75 Hz, $H_{2′,6′}$), 7.45 (d, 2H, J = 8.75 Hz, $H_{3′,5′}$), 7.7 (broad, 1H, NH), 7.73 (s, 1H, OH); ^{13}C NMR ($CDCl_3$) δ 182.87 (C_1), 182.11 (C_4), 153.49 (C_3), 142.96 (C_6), 138.6 ($C_{4′}$), 130.99 (C_{13}), 131.55 ($C_{3′,5′}$); 127.98 (C_2), 124.82 (C_{12}), 123.31 ($C_{2′,6′}$), 118.98 (C_5), 116.40 ($C_{1′}$), 34.12 (C_{10}), 29.4 (C_9), 26.42 (C_{15}), 26.29 (C_{11}), 18.3 (C_8), 17.82 (C_{14}), 12.07 (C_7); MS *m*/*z* 417, 418, 419, 421, 360, 338, 336, 335, 309, 257, 180, 149, 334, 308. Anal. Calcd for $C_{21}H_{24}O_3N$; C, 60.28; H, 5.74; N, 3.34; Br, 19.13. Found: C, 60.51; H, 5.47; N, 3.33; Br, 19.27.

2-(1,5-Dimethyl-4-hexenyl)-3-hydroxy-7-[(4′-acetylphenyl)-amine]-1,4-benzoquinone (*p*-MeCOAPZ). A 0.304 g portion of 4-aminoacetophenone yielded 0.690 g (90%) of the desired product: mp 115−116 °C; UV−vis (MeOH, nm) 522, 316, 204; ^{1}H NMR ($CDCl_3$) δ 1.2 (d, 3H, J = 7.0 Hz, H_8), 1.5 (s, 3H, H_7), 1.55 (s, 3H, H_{14}), 1.6 (m, 1H, H_{10}), 1.65 (d, 3H, J = 1.0 Hz, H_{15}), 1.8 (m, 1H, H_{10}), 1.9 (m, 2H, H_{11}), 2.74 (s, 1H, R_2), 3.05 (dq, 1H, J = 8.7, 7.2 Hz, H_9), 5.1 (ts, 1H, J = 1.2, 7.2 Hz, H_{12}), 6.9 (d, 2H, J = 8.6 Hz, $H_{3′,5′}$), 7.4 (broad, 1H, NH), 7.5 (d, 2H, J = 8.6 Hz, $H_{2′,6′}$), 7.8 (s, 1H, OH); ^{13}C NMR ($CDCl_3$) δ 195.79 (R_2), 182.96 (C_1), 182.27 (C_4), 153.37 (C_3), 142.85 (C_6), 138.5 ($C_{4′}$), 131.16 ($C_{1′}$), 131.03 (C_{13}), 129.44 (C_2), 128.79 ($C_{3′,5′}$), 124.68 (C_{12}), 119.23 (C_5), 119.22 ($C_{2′,6′}$), 33.95 (C_{10}), 29.4 (C_9), 26.5 (C_{15}), 26.01 (C_{11}), 18.3 (C_8), 17.73 (C_{14}), 12.35 (C_7); MS *m*/*z* 381, 339, 324, 310, 300, 299, 273, 229, 226, 191, 158, 113, 111, 272, 257, 157, 135. Anal. Calcd for $C_{24}H_{27}O_4N$; C, 72.44; H, 7.08; N, 3.67. Found: C, 72.54; H, 7.08; N, 3.64.

2-(1,5-Dimethyl-4-hexenyl)-3-hydroxy-5-methyl-6-[(4′-cyanophenyl)amine]-1,4-benzoquinone (*p*-CNAPZ). A 0.237 g portion of 4-aminobenzonitrile yielded 0.622 g (85%) of the desired product: mp 93−95 °C; IR (KBr, cm^{-1}) 3336, 3280, 2966, 2926, 2862, 2224, 1638, 1597, 1572, 1510, 1484, 1374, 1317, 1284, 1172, 1113, 1091, 828, 763, 697, 627, 550; UV−vis (MeOH, nm) 513, 354, 281, 209; ^{1}H NMR ($CDCl_3$) δ 1.22 (d, 3H, J = 7.0 Hz, H_8), 1.55 (s, 3H, H_{14}), 1.58 (m, 1H, H_{10}), 1.63 (s, 3H, H_7), 1.65 (d, 3H, J = 1.2 Hz, H_{15}), 1.8 (m, 1H, H_{10}), 1.92 (m, 2H, H_{11}), 3.07 (dq, 1H, J = 7.2, 8.7 Hz, H_9), 5.08 (ts, 1H, J = 1.2, 7.2 Hz, H_{12}), 6.98 (d, 2H, J = 8.6 Hz, $H_{2′,6′}$), 7.63 (d, 2H, J = 8.6 Hz, $H_{3′,5′}$), 7.75 (broad, 1H, NH), 7.8 (s, 1H, OH); ^{13}C NMR ($CDCl_3$) δ 183.45 (C_1), 182.49 (C_4), 152.91 (C_3), 141.10 (C_6), 143.16 ($C_{4′}$), 131.47 (C_2, C_{13}), 133.04 ($C_{3′,5′}$), 124.33 (C_{12}), 121.63 ($C_{2′,6′}$), 120.21 (C_5), 118.58 (R_2), 111.85 ($C_{1′}$), 34.07 (C_{10}), 29.64 (C_9), 26.59 (C_{11}), 25.67 (C_{15}), 18.26 (C_8), 17.61 (C_{14}), 13.21 (C_7); MS *m*/*z* 364, 335, 322, 321, 307, 282, 253, 239, 180, 117, 155, 109. Anal. Calcd for $C_{22}H_{24}N_2O_3$; C, 72.53; H, 6.59; N, 7.69. Found: C, 72.40; H, 6.53; N, 7.60.

2-(1,5-Dimethyl-4-hexenyl)-3-hydroxy-5-methyl-6-[(4′-nitrophenyl)amine]-1,4-benzoquinone (*p*-NO_2APZ). A 0.277 g portion of 4-nitroaniline yielded 0.310 g (40%) of the desired product: mp 132−135 °C; IR ($CHCl_3$, cm^{-1}) 832, 852, 922, 1013, 1058, 1091, 1113, 1178, 1262, 1279, 1303, 1341, 1378, 1398, 1453, 1507, 1591, 1619, 1643, 1711, 1723, 2857, 2929, 2965, 3326; UV−vis (MeOH, nm) 501, 368, 273, 205; ^{1}H NMR ($CDCl_3$) δ 1.21 (d, 3H, J = 7.0 Hz, H_8), 1.54 (s, 3H, H_{14}), 1.6 (m, 1H, H_{10}), 1.65 (s, 3H, H_7), 1.65 (d, 4H, J = 1.0 Hz, H_{15}), 1.8 (m, 1H, H_{10}), 1.9 (m, 2H, H_{11}), 3.05 (dq, 1H, J = 7.0, 8.5 Hz, H_9), 5.09 (ts, 1H, J = 1.5, 7.0 Hz, H_{12}), 6.95 (d, 2H, J = 9.0 Hz, $H_{2′,6′}$), 7.6 (broad, 1H, NH), 7.7 (s, 1H, OH), 8.18 (d, 2H, J = 9 Hz, $H_{3′,5′}$); ^{13}C NMR ($CDCl_3$) δ 183.05 (C_1), 182.44 (C_4), 153.25 (C_3), 142.74 (C_6), 141.5 (C_{19}), 137.77 ($C_{1′}$), 131.06 (C_{13}), 130.96 (C_2), 124.53 (C_{12}), 124.2 ($C_{3′,5′}$), 119.5 (C_5), 118.29 ($C_{2′,6′}$), 33.76 (C_{10}), 29.5 ($C_{4′}$), 26.59 (C_{15}), 25.72 (C_{11}), 18.4 (C_8), 17.63 (C_{14}), 12.65 (C_7); MS *m*/*z* 384, 341, 327, 303, 302, 249, 248, 247, 177, 166, 165, 146, 106. Anal. Calcd for $C_{21}H_{24}O_5N_2$; C, 65.62; H, 6.25; N, 364. Found: C, 65.70; H, 6.19; N, 3.92.

General Procedure (II) for the Synthesis of Substituted 2-(1,5-Dimethyl-4-hexenyl)-3-methoxy-5-methyl-6-[4′-(R_2-phenyl)amine]-1,4-benzoquinones (APZms). A 4 g portion of sodium carbonate and 1.5 mmol of recently distilled dimethyl sulfate (1.5 mmol, 0.189 g) were added to a solution of 1.0 mmol of APZs in 25 mL of anhydrous acetone in a dry flask. The reaction mixture was refluxed for 12 h. After the mixture was cooled, 10 mL of 2 N KOH was added and the solvent was removed in a vacuum. The residue was dissolved in ethyl acetate (50 mL), and the organic phase was washed with water and brine and then dried over Na_2SO_4. After the solvent was evaporated, the residue was subjected to column chromatography (silica gel, *n*-hexane−ethyl acetate 9:1) yielding the desired product.

2-(1,5-Dimethyl-4-hexenyl)-3-methoxy-5-methyl-1,4-benzoquinone (PZm). A 0.248 g portion of PZ under general procedure II yielded 0.236 g (90%) of the desired product as a yellow oil:[21] IR ($CHCl_3$, cm^{-1}) 2965, 2928, 2856, 1655, 1636, 1599, 1449, 1377, 1273, 1057, 926, 889; UV−vis (MeOH, nm) 373, 262.5, 207; ^{1}H NMR ($CDCl_3$) δ 1.18 (d, 3H, J = 7.0 Hz, H_8), 1.54 (s, 3H, H_{15}), 1.59 (m, 1H, H_{10}), 1.65 (d, 3H, J = 1.5 Hz, H_{14}), 1.75 (m, 1H, H_{10}), 1.89 (m, 2H, H_{11}), 2.01 (s, 3H, H_7), 3.09 (dq, 1H, J = 7.0, 8.5 Hz, H_9), 3.95 (s, 3H, OMe), 5.06 (ts, 1H, J = 1.5, 7.02 Hz, H_{12}), 6.47 (q, 1H, H_6); MS *m*/*z* 262, 247, 219, 205, 180, 165, 161, 137, 109, 91, 69, 55, 41, 28, 18, 17. Anal. Calcd for $C_{16}H_{22}O_3$: C, 73.28; H, 8.45. Found: C, 73.14; H, 8.62.

2-(1,5-Dimethyl-4-hexenyl)-3-methoxy-5-methyl-6-[(4′-methoxyphenyl)amino]-1,4-benzoquinone (*p*-MeOAPZm). A 0.370 g portion of the methoxy derivative (PZm) reacted according to general procedure II. After column purification, 0.345 g (90% yield) of deep blue oil was obtained: IR ($CHCl_3$, cm^{-1}) 3335, 2936, 2842, 1643, 1593, 1512, 1462, 1339, 1270, 1200, 1115; UV−vis (MeOH, nm) 543, 290, 257, 209; ^{1}H NMR ($CDCl_3$) δ 1.2 (d, 3H, J = 7.0 Hz, H_8), 1.50 (S, 3H, H_{15}), 1.56 (s, 3H, H_7), 1.60 (m, 1H, H_{10}), 1.66 (d, 3H, J = 1.0 Jz, H_{14}), 1.77 (m, 1H, H_{10}), 1.92 (m, 2H, H_{11}), 3.11 (dq, 1H, J = 7.0, 9.0 Hz, H_9), 3.81 (s, 3H, R_2), 4.04 (s, 3H, OMe), 5.09 (ts, 1H, J = 1.5, 7.0 Hz, H_{12}), 6.85 (d, 2H, J = 9 Hz, $H_{2′,6′}$), 6.94 (d, 2H, J = 9.0 Hz, $H_{3′,5′}$), 7.23 (broad, 1H, NH); ^{13}C NMR ($CDCl_3$) δ 185.01 (C_1), 183.07 (C_4), 158.22 (C_3), 156.93 (C_6), 141.16 ($C_{4′}$), 132.64 ($C_{1′}$), 131.44 (C_2), 131.22 (C_{13}), 125.02 ($C_{3′,5′}$), 125.57 (C_{12}), 114.0 ($C_{2′,6′}$), 110.26 (C_5), 61.40 (OMe), 55.46 (R_2) 34.65 (C_{10}), 29.60 (C_9), 26.78 (C_{11}), 25.66 (C_{14}), 18.88 (C_8), 17.65 (C_{15}), 11.84 (C_7); MS *m*/*z* 383, 368, 352, 340, 301, 273, 248, 233, 205, 193, 167, 166, 149, 123, 108, 77, 69, 41, 39. A FAB^+ ion mass spectrum showed M^+ peak at 383.2101 (calcd parent peak 383.2097) for $C_{23}H_{29}O_4N$: C, 72.06; H, 7.57; O, 16.71; N, 3.66. Anal. Calcd for $C_{23}H_{29}O_4N$: C, 72.06; H, 7.57; N, 3.66. Found: C, 71.98; H, 7.48; N, 3.60.

2-(1,5-Dimethyl-4-hexenyl)-3-methoxy-5-methyl-6-[(4′-methylphenyl)amine]-1,4-benzoquinone (*p*-MeAPZm). According to general procedure II, 0.350 g of *p*-MeAPZ yielded 0.338 g (92%) of a deep blue oil: IR (film, cm^{-1}) 3324, 2960, 2926, 2858, 1644, 1594, 1517, 1492, 1451, 1376, 1315, 1289, 1262, 1119, 1098, 1062; UV−vis (MeOH, nm) 535, 260, 210; ^{1}H NMR ($CDCl_3$) δ 1.18 (d, 3H, J = 7.0 Hz, H_8), 1.53 (s, 3H, H_7), 1.56 (s, 3H, H_{15}), 1.6 (m, 1H, H_{10}), 1.66 (d, 3H, J = 1.5 Hz, H_{14}), 1.76 (m, 1H, H_{10}), 1.91 (m, 2H, H_{11}), 2.33 (s, 3H, R_2), 3.12 (dq, 1H, J = 7.0, 8.5 Hz, H_9), 4.04 (s, 3H, OMe), 5.08 (ts, 1H, J = 1.5, 7.0 Hz, H_{12}), 6.86 (d, 2H, J = 8.0 Hz, $H_{2′,6′}$), 7.11 (d, 2H, J = 8.0 Hz, $H_{3′,5′}$), 7.23 (broad, 1H, NH); ^{13}C NMR ($CDCl_3$) δ 185.04 (C_1), 183.14 (C_4), 158.1 (C_3), 140.70 (C_6), 134.11 ($C_{4′}$), 129.32 ($C_{3′,5′}$), 131.41 (C_2, C_{13}), 124.52 (C_{12}), 122.83 ($C_{2′,6′}$), 137 ($C_{1′}$), 111.35 (C_5), 61.38 (OMe), 34.65 (C_{10}), 29.61 (C_9), 26.78 (C_{11}), 25.67 (C_{14}), 20.84 (R_2) 18.9, (C_8), 17.67 (C_{15}), 12.35 (C_7); MS *m*/*z* 367, 352, 336, 324, 298, 285, 270, 257, 242, 226, 183, 181, 180, 149, 144, 118. A FAB^+ ion mass spectrum showed M^+ peak at 368.2224 (calcd parent peak 368.2226) for $C_{23}H_{29}O_3N$: C, 75.2; H, 7.9; 0, 13.08; N, 3.82. Anal. Calcd for $C_{23}H_{29}O_3N$; C, 75.20; H, 7.90; N, 3.81. Found: C, 75.13; H, 7.87; N, 3.76.

2-(1,5-Dimethyl-4-hexenyl)-3-methoxy-6-phenylamine-1,4-benzoquinone (APZm). A 0.340 g portion of APZ reacted according to general procedure II. After column purification, 0.30 g (85% yield) of deep blue oil was obtained: IR ($CHCl_3$, cm^{-1}) 3339, 2966, 2934, 2858, 1645, 1589, 1506, 1449, 1377, 1315, 1173, 1097, 1061, 1022, 941, 895; UV−vis 526, 321, 261, 207; ^1H NMR ($CDCl_3$) δ 1.21 (d, 3H, $J = 7.0$ Hz, H_8), 1.55 (s, 6H, H_7, H_{15}), 1.6 (m, 1H, H_{10}), 1.66 (d, 3H, $J = 1.5$ Hz, H_{14}), 1.76 (m, 1H, H_{10}), 1.92 (m, 2H, H_{11}), 3.12 (dq, 1H, $J = 7.0$, 8.5 Hz, H_9), 4.04 (s, 3H, OMe), 5.08 (ts, 1H, $J = 1.5$, 7.0 Hz, H_{12}), 6.95 (d, 2H, $J = 7.5$ Hz, $H_{2',6'}$), 7.1 (t, 1H, R_2), 7.28 (broad, 1H, NH), 7.3 (d, 2H, $J = 7.5$ Hz, $H_{3',5'}$); ^{13}C NMR ($CDCl_3$) δ 185.04 (C_1), 183.29 (C_4), 158.04 (C_3), 140.46 (C_6), 139.70 ($C_{4'}$), 128.81 ($C_{3',5'}$), 131.65 (C_2, C_{13}), 124.54 (C_{12}), 122.45 ($C_{2',6'}$), 124.14 ($C_{1'}$), 112.51 (C_5), 61.40 (OMe), 34.67 (C_{10}), 29.65 (C_9), 26.79 (C_{11}), 25.67 (C_{14}), 18.89 (C_8), 17.67 (C_{15}), 12.61 (C_7); MS *m/z* 353, 338, 310, 306, 284, 271, 243, 228, 226, 198, 184, 166, 158, 130, 109, 93, 77, 69, 41, 39, 27, 15. A FAB^+ ion mass spectrum showed M^+ peak at 354.2061 (calcd parent peak 354.2069) for $C_{22}H_{28}O_3N$: C, 74.79; H, 7.65; O, 13.60; N, 3.96. Anal. Calcd for $C_{22}H_{27}O_3N$; C, 74.85; H, 7.65; N, 3.97. Found: C, 74.78; H, 7.60; N, 3.85.

2-(1,5-Dimethyl-4-hexenyl)-3-methoxy-5-methyl-6-[(4′-bromophenyl)amine]-1,4-benzoquinone (*p*-BrAPZm). According to general procedure II, 0.420 g of *p*-BrAPZ yielded 0.300 g (71%) of a blue oil: IR (film, cm^{-1}) 3337, 2963, 2932, 2856, 1643, 1599, 1500, 1454, 1377, 1299, 1261, 1097, 1013; UV−vis (MeOH, nm) 520, 328, 268, 208; ^1H NMR ($CDCl_3$) δ 1.2 (d, 3H, $J = 7.0$ Hz, H_8), 1.55 (s, 3H, H_{15}), 1.56 (s, 3H, H_7), 1.6 (m, 1H, H_{10}), 1.65 (d, 3H, $J = 1.5$ Hz, H_{14}), 1.76 (m, 1H, H_{10}), 1.91 (m, 2H, H_{11}), 3.12 (dq, 1H, $J = 7.0$, 8.5 Hz, H_9), 4.04 (s, 3H, OMe), 5.08 (ts, 1H, $J = 1.5$, 7.0 Hz, H_{12}), 6.9 (d, 2H, $J = 8.75$ Hz, $H_{2',6'}$), 7.18 (broad, 1H, NH), 7.42 (d, 2H, $J = 8.75$ Hz, $H_{3',5'}$); ^{13}C NMR ($CDCl_3$) δ 184.82 (C_1), 183.28 (C_4), 157.93 (C_3), 140.08 (C_6), 138.9 ($C_{4'}$), 131.85 ($C_{3',5'}$), 131.53 (C_2, C_{13}), 124.47 (C_{12}), 123.60 ($C_{2',6'}$), 116.7 ($C_{1'}$), 113.41 (C_5), 61.41 (OMe), 34.64 (C_{10}), 29.0 (C_9), 26.7 (C_{11}), 25.66 (C_{14}), 18.85 (C_8), 17.66 (C_{15}), 12.82 (C_7); MS *m/z* 433, 431, 401, 388, 351, 349, 321, 306, 279, 256, 227, 226, 210, 167, 149, 130, 109, 93.69. A FAB^+ ion mass spectrum showed M^+ peak at 433.1264 (calcd parent peak 433.1253) for $C_{22}H_{26}O_3NBr$: C, 61.11; H, 6.02; O, 11.11; N, 3.24; Br, 18.52. Anal. Calcd for $C_{22}H_{26}O_3NBr$; C, 61.11; H, 6.02; N, 3.24. Found: C, 60.98; H, 5.98; N, 3.19.

2-(1,5-Dimethyl-4-hexenyl)-3-methoxy-5-methyl-6-[(4′-acetylphenyl)amine]-1,4-benzoquinone (*p*-MeCOAPZm). A 0.380 g portion of the *p*-MeCOAPZ reacted according to general procedure II. After column purification, 0.328 g (83% yield) of blue oil was obtained: IR (film, cm^{-1}) 3318, 2961, 2927, 2856, 1676, 1645, 1593, 1517, 1492, 1449, 1412, 1358, 1309, 1259, 1177, 1121, 1097, 1062, 1013, 957, 829, 760; UV−vis (MeOH, nm) 510, 313, 225.5, 207; ^1H NMR ($CDCl_3$) δ 1.21 (d, 3H, $J = 7.0$ Hz, H_8), 1.55 (s, 3H, H_{15}), 1.65 (s, 3H, H_7), 1.6 (m, 1H, H_{10}), 1.65 (d, 3H, $J = 1.0$ Hz, H_{14}), 1.76 (m, 1H, H_{10}), 1.92 (m, 2H, H_{11}), 3.13 (dq, 1H, $J = 8.7$, 7.2 Hz, H_9), 2.5 (s, 1H, R_2), 4.06 (s, 3H, OMe) 5.07 (ts, 1H, $J = 1.2$, 7.2 Hz, H_{12}), 6.89 (d, 2H, $J = 8.6$ Hz, $H_{2',6'}$), 7.93 (d, 2H, $J = 8.6$ Hz, $H_{3',5'}$), 7.36 (broad, 1H, NH); ^{13}C NMR ($CDCl_3$) δ 199.56 (R_2), 184.74 (C_1), 183.36 (C_4), 157.71 (C_3), 144.23 (C_6), 139.27 ($C_{4'}$), 131.93 ($C_{1'}$), 132.32 (C_2) 131.56 (C_{13}), 129.56 ($C_{3',5'}$), 124.40 (C_{12}), 119.99 ($C_{2',6'}$), 116.54 (C_5), 61.41 (OMe), 34.65 (C_{10}), 29.73 (C_9), 26.78 (C_{11}), 26.38 (R_2), 25.69 (C_{14}), 18.85 (C_8), 17.68 (C_{15}), 13.41 (C_7); MS *m/z* 395, 364, 352, 313, 285, 270, 256, 228, 197, 180, 167, 149, 109, 83. A FAB^+ ion mass spectrum showed M^+ peak at 396.2191, (calcd parent peak 396.2175) for $C_{24}H_{29}O_4N$: C, 72.91; H, 7.34; O, 162.2; N, 3.54. Anal. Calcd for $C_{24}H_{29}O_4N$; C, 72.91; H, 7.34; N, 3.54. Found: C, 72.81; H, 7.29; N, 3.50.

2-(1,5-Dimethyl-4-hexenyl)-3-methoxy-5-methyl-6-[(4′-cyanophenyl)amine]-1,4-benzoquinone (*p*-CNAPZm). According to general procedure II, 0.360 g of *p*-CNAPZ yielded 0.320 g (85%) of blue oil: IR ($CHCl_3$, cm^{-1}) 3339, 2967, 2931, 2855, 2228, 1644, 1597, 1514, 1492, 1458, 1363, 1315, 1121; UV−vis (MeOH, nm) 503.5, 283.5, 208.0; ^1H NMR ($CDCl_3$) δ 1.2 (d, 3H, $J = 7.0$ Hz, H_8), 1.55 (s, 3H, H_{15}), 1.57 (s, 3H, H_7), 1.61 (m, 1H, H_{10}), 1.65 (d, 3H, $J = 1.2$ Hz, H_{14}), 1.75 (m, 1H, H_{10}), 1.9 (m, 2H, H_{11}), 3.13 (dq, 1H, $J = 7.2$, 8.7 Hz, H_9), 4.05 (s, 3H, OMe), 5.07 (ts, 1H, $J = 1.2$, 7.2 Hz, H_{12}), 6.88 (d, 2H, $J = 8.6$ Hz, $H_{2',6'}$), 7.27 (broad, 1H, NH), 7.59 (d, 2H, $J = 8.6$ Hz, $H_{3',5'}$); ^{13}C NMR ($CDCl_3$) δ 184.58 (C_1), 183.35 (C_4), 157.64 (C_3), 144.03 (C_6), 138.84 ($C_{4'}$), 133.13 ($C_{3',5'}$), 132.6 (C_2), 131.62 (C_{13}), 124.37 (C_{12}), 120.21 ($C_{2',6'}$), 118.85 (R_2), 117.74 ($C_{1'}$), 105.71 (C_5), 61.41 (OMe), 34.62 (C_{10}), 29.73 (C_9), 26.75 (C_{11}), 25.66 (C_{14}), 18.81 (C_8), 17.66 (C_{15}), 13.48 (C_7); MS *m/z* 378, 347, 335, 309, 296, 268, 253, 251, 209, 183, 178, 155, 119, 109, 102, 69. A FAB^+ ion mass spectrum showed M^+ peak at 378.1958 (calcd parent peak 378.1943) for $C_{23}H_{26}O_3N_2$: C, 73.02; H, 6.88; O, 12.70; N, 7.40. Anal. Calcd for $C_{23}H_{26}O_3N$; C, 73.02; H.6.88; N, 7.40. Found: C, 72.94; H 6.63; N, 7.35.

2-(1,5-Dimethyl-4-hexenyl)-3-methoxy-5-methyl-6-[(4′-nitrophenyl)amine]-1,4-benzoquinone (*p*-NO_2APZm). According to general procedure II, 0.380 g of *p*-NO_2APZ yielded 0.260 g (65%) of a deep red oil: IR ($CHCl_3$, cm^{-1}) 3339, 2963, 2934, 2856, 1645, 1591, 1506, 1452, 1377, 1339, 1304, 1113, 1009; UV−vis (MeOH, nm) 491, 348, 274, 230, 210; ^1H NMR ($CDCl_3$) δ 1.21 (d, 3H, $J = 7.0$ Hz, H_8), 1.55 (s, 3H, H_{15}), 1.69 (s, 3H, H_7), 1.61 (m, 1H, H_{10}), 1.65 (d, 3H, $J = 1.0$ Hz, H_{14}), 1.75 (m, 1H, H_{10}), 1.92 (m, 2H, H_{11}), 3.14 (dq, 1H, $J = 7$, 8.5 Hz, H_9), 4.06 (s, 3H, OMe), 5.07 (ts, 1H, $J = 1.5$ 7.0 Hz, H_{12}), 6.88 (d, 2H, $J = 9.0$ Hz, $H_{2',6'}$), 7.38 (broad, 1H, NH), 8.02 (d, 2H, $J = 9.0$ Hz, $H_{3',5'}$); ^{13}C NMR ($CDCl_3$) δ 184.51 (C_1), 183.36 (C_4), 157.61 (C_3), 145.93 (C_6), 142.44 ($C_{4'}$), 125.14 ($C_{3',5'}$), 132.76 (C_2), 131.66 (C_{13}), 124.35 (C_{12}), 119.23 ($C_{2',6'}$), 138.71 ($C_{1'}$), 118.84 (C_5), 61.42 (OMe), 34.61 (C_{10}), 29.75 (C_9), 26.75 (C_{11}), 25.66 (C_{14}), 18.80 (C_8), 17.66 (C_{15}), 13.60 (C_7); MS *m/z* 398, 383, 355, 316, 301, 288, 262, 248, 227, 180, 179, 165, 109. A FAB^+ ion mass spectrum showed $M^+ + 1$ peak at 399.1939 (calcd parent peak 399.1920) for $C_{22}H_{26}O_5N_2$: C, 66.33; H, 6.53; O, 20.1; N, 7.04. Anal. Calcd for $C_{22}H_{26}O_5N_2$: C, 66.33; H, 6.53; N, 7.04. Found: C, 66.15; H, 6.48; N, 6.93.

X-ray Procedure. Suitable crystals of APZ were grown by slow evaporation from a *n*-hexane/ethyl acetate solution at room temperature. A summary of data collection and refinement conditions are given in Figure S1 (Supporting Information). Intensities were collected on a Siemens P4/PC diffractrometer using a ω-scan, with Mo Kα radiation. The structures were solved by direct methods and refined by a full-matrix least-squares procedure.[49]

Hydrogen atoms were included at idealized geometric positions and forced to ride on the carbon parent atom. Only hydrogen atoms related to hydrogen bonds were refined. See the Supporting Information for details.

Electrochemical Procedure. Solvent and Supporting Electrolyte. Acetonitrile (AN) (Aldrich) was dried overnight with $CaCl_2$ (Merck) and purified by distillation on P_2O_5 (Merck) under vacuum. Traces of water in the solvent were eliminated by contact with a 3 Å molecular sieve (Merck) in the dark. The absence of the characteristic −OH bands in the IR spectra confirmed the completed elimination of water traces. Tetraethylammonium tetrafluoroborate (Et_4NBF_4) (Fluka) was dried under vacuum at 60 °C.

Electrodes, Apparatus, and Instrumentation. Cyclic voltammetry measurements were carried out in a conventional three-electrode cell. A polished glassy 7 mm^2 area carbon-disk electrode was used as a working electrode. Prior to measurements, this electrode was cleaned and polished with 0.05 μm alumina (Buehler), wiped with a tissue, and sonicated in distilled water for 2−4 min. A platinum wire served as the counter electrode. The reference electrode was an aqueous saturated calomel electrode (SCE), isolated from the main cell body by a Luggin tube filled with 0.1 M Et_4NBF_4/acetonitrile.

Peak potentials were measured at controlled temperature (25 °C) in acetonitrile solutions using 0.1 M Et_4NBF_4 as the supporting electrolyte. APZs and APZms solutions (1.0 mM) were used. At lower concentrations of the electroactive species the current capacitive precluded acceptable evaluation of current peaks. $Me_4N^+C_6H_5O^-$ was prepared with equimolar

(49) (a) Altomare, G.; Cascarano, C.; Giacovazzo, A.; Guagliardi, M. C.; Burla, G.; Polidori, M.; Camalli, J. *J. Appl. Crystallogr.* **1994**, 27, 435. (b) Sheldrick, G. M. SHELLXL93. Program for Refinement of Crystal Structures. University of Göttingen, Germany, 1993.

quantities of phenol and 0.1 M tetramethylammonium hydroxide. For cyclic voltammetric experiments, 2 mM $Me_4N^+C_6H_5O^-$ was added to the electrolytic medium. Voltammetric curves were recorded using a BAS 100B/W Electrochemical Analyzer of Bioanalytical Systems interfaced with a Gateway 2000 personal computer. Measurements were made over a potential range between 250 and −2500 mV with a sweep rate of 50−9000 mVs^{-1}. Prior to the experiments, solutions were purged with nitrogen, which was presaturated with the appropriate solvent containing 3 Å sieves. All potentials were determined under the same conditions to obtain a consistent data set. To establish a reference system with the experimental conditions of our particular system, the redox potentials reported in this paper refer to the ferrocene/ferrocinium (Fc/Fc^+) pair, as recommended by IUPAC.[50] In this case, the potential for the ferrocene/ferrocinium (Fc/Fc^+) redox pair, determined by voltamperometric studies, was 412 mV vs SCE.

Computational Methods. Full geometry optimization (without symmetry constraints) on the model structures of perezone derivatives was performed at the B3LYP/6-31G(d,p) level with the Gaussian 94 Program (G94).[31] The Becke3LYP hybrid functional defines the exchange function as a linear combination of Hartree−Fock, local, and gradient-corrected terms.[51] The exchange function is combined with a local and gradient-corrected correlation function.

The correlation function used was C*EcLYP + (1 − c) − *EcVWN, where LYP is the correlation functional of Lee, Yang and Parr,[52] and includes both local and nonlocal terms, and VWN is the Vosko, Wilk, and Nusair 1980 correlation functional fitting the RPA solution to the uniform gas, often referred to as local spin density (LSD) correlation.[53] VWN was used to provide the excess of the local correlation, required since LYP contains a local term essentially equivalent to VWN.[42,54]

The orbital basis set, 6-31G(d,p), was used to add polarization functions to heavy atoms and hydrogens. Natural bond orbital analyses (NBO) were carried out with version 3.1, which is included in G94. Densities computed at B3LYP/6-31G(d,p) level from the G94 output were used with the AIMPAC[33] set of programs to calculate the properties of critical points (cps) in the charge density (ρ), Laplacians ($\nabla^2\rho$), and ellipticities (ϵ).

Acknowledgment. We are grateful to the Dirección General de Servicios de Cómputo Académico, Universidad Nacional Autónoma de México, DGSCA, UNAM, and to the Escuela de Ciencias Químicas, Universidad La Salle, for their computational support as well as for the generous gift of supercomputer CPU time. We also thank the Consejo Nacional de Ciencia y Tecnología (CONACyT) for financial support given as Grant Nos. 32420-E and 28016-E and fellowships to N.M.-R., J.A.B.-M., E.T., and T.M.A. N.M.-R. and J.A.B.-M. are also grateful to DGEP for a complementary fellowship. We are grateful to Sylvain Bernes for the X-ray structure determination, to Luis Velasco and Francisco Pérez Flores for the mass spectral determination, and Ma. del Rocio Patiño and to Isabel Chavez for technical support.

Supporting Information Available: Tables of the crystal data and structure refinement information, bond lengths and bond angles, atomic and hydrogen coordinates, and isotropic and anisotropic displacement coordinates for APZ. This material is available free of charge via the Internet at http://pubs.acs.org.

JO010302Z

(50) Gritzner, G.; Küta, J. *Pure Appl. Chem.* **1984**, *4*, 462−466.

(51) (a) Stephens, P. J.; Devlin, F. J.; Chabalowski, C. F.; Frisch, M. J. *J. Phys. Chem.* **1994**, *98*, 11623−11627. (b) Becke, A. D. *J. Chem. Phys.* **1993**, *98*, 1372−1377, 5648−5652.

(52) (a) Lee, C.; Yang, W.; Parr, R. G.; *Phys. Rev.* **1988**, *B37*, 785−789. (b) Miehlich, B.; Savin, A.; Stoll, H.; Preuss, H. *Chem. Phys. Lett.* **1989**, *157*, 200−206.

(53) Vosko, S. H.; Wilk, L.; Nusair, M. *Can. J. Phys.* **1980**, *58*, 1200−1211.

(54) (a) Becke, A. D. *J. Chem. Phys.* **1988**, *88*, 1053−1062. (b) Becke, A. D. *Phys. Rev. A.* **1988**, *38*, 3098−3100.